Journal of Chemical&Engineering Data

Open Access
This article is licensed under CC-BY 4.0

pubs.acs.org/jced
Article

Tailoring Deep Eutectic Solvents: The Role of Hydrated Metal Salts in Modifying Structural Organization and Macroscopic Performance

Guadalupe Pérez-Durán, Hamza I. Hossain, Enrique Muñoz-Quintana, Luis Antonio Castillo-Felix, Supti Paul, Santiago Aparicio, Alberto Gutiérrez-Vega, Gustavo A. Iglesias-Silva,* and Mert Atilhan*

Cite This: J. Chem. Eng. Data 2026, 71, 2914−2931

Read Online
ACCESS | Metrics & More | Article Recommendations

ABSTRACT: Deep eutectic solvents (DES) have emerged as promising green alternatives to conventional solvents; however, their broader implementation remains limited by the scarcity of reliable thermophysical and interfacial property data, particularly for multicomponent systems. In this work, a systematic experimental characterization was carried out on a ternary DES based on ChCl:Gly (1:2) incorporating hydrated metal salts. Systems containing $AlCl_3{\cdot}6H_2O$, $MgCl_2{\cdot}6H_2O$, $Mg(NO_3)_2{\cdot}6H_2O$, and $CaCl_2{\cdot}2H_2O$ are prepared at metal salt molar fractions ranging from 0.10 to 0.35. Density, viscosity, speed of sound, surface tension, and contact angle are measured over the temperature range of 293.15−343.15 K at atmospheric pressure. Experimental density, viscosity, and speed-of-sound data were correlated using empirical regression models, providing accurate descriptions of their temperature dependence and enabling predictive capability. Surface tension and contact angle measurements are used to assess interfacial behavior and wettability, revealing clear dependencies on DES composition and substrate nature. Overall, this work provides a consistent data set of bulk and interfacial properties for these choline chloride:glycerol:metal salt hydrated DES systems, contributing to improved structure−property understanding and supporting their rational design and application in process-oriented systems.

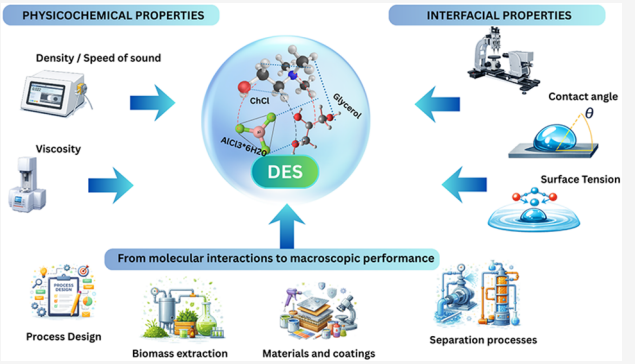

1. INTRODUCTION

Deep eutectic solvents (DES), including variants such as natural deep eutectic solvents (NADES), low transition temperature mixtures (LTTM), and mixtures of natural compounds, have recently emerged as a promising class of green designer solvents for diverse applications.[1] DES are formed by mixing a hydrogen-bond acceptor (HBA) and a hydrogen-bond donor (HBD), resulting in a eutectic mixture with a melting point significantly lower than that of the individual components.[2] Originally conceived as more sustainable analogues of ionic liquids (ILs), DES have attracted widespread attention due to their negligible vapor pressure, high thermal stability, and tunable physicochemical properties. In addition to sharing key advantages with ILs, DES offer further benefits such as simple preparation, low cost, and enhanced biocompatibility, as they are often composed of nontoxic, biodegradable, and readily available components.[3] Accordingly, these novel solvents have attracted significant interest due to their favorable and distinctive characteristics. They have been widely explored as environmentally friendly solvents for applications in electrochemistry,[4] biomass processing,[5,6] and related fields. In many cases, DES are proposed as sustainable alternatives to conventional volatile organic solvents, or even to ILs, in industrially relevant processes such as extraction, separation, CO_2 capture,[7] metal recovery,[8] chromatography,[9] biodiesel production,[10] and drug delivery.[11] Studies on deep eutectic solvents (DES) based upon hydrated salts remain limited. Marcus[12] provides a comprehensive review of unconventional DES formed from hydrated salts, reporting physical properties for 25 systems primarily composed of water (or ice) and hydrated salts. A limited number of binary DES systems have also been described, including $Zn(NO_3)_2{\cdot}6H_2O$ + urea, $CaCl_2{\cdot}6H_2O$ + choline chloride, and $CrCl_3{\cdot}6H_2O$ + urea. To the best of our knowledge, no data have been reported for the physical properties of ternary DES containing hydrated salts.

Although research on deep eutectic solvents (DES) has increased rapidly in recent years, a comprehensive understanding of their physicochemical properties and internal

Received: March 10, 2026
Revised: June 2, 2026
Accepted: June 9, 2026
Published: June 17, 2026

ACS Publications
© 2026 The Authors. Published by American Chemical Society

https://doi.org/10.1021/acs.jced.6c00151
J. Chem. Eng. Data 2026, 71, 2914−2931

Downloaded from pubs.acs.org/jceaax/article-pdf/71/7/2914/6510546/acs.jced.6c00151.pdf by UNIV DE BURGOS user on 07 September 2026

Table 1. Specifications of the Samples

chemical	abbreviation	CAS No.	lot	manufacturer	purity (%)
choline chloride	ChCl	67−48−1	A0438363	Thermo Scientific	99
glycerol	Gly	56−81−5	G7893−1L	Sigma-Aldrich	99.5
magnesium chloride hexahydrate	$MgCl_2·6H_2O$	7791−18−6	A0460941	Thermo Scientific	99
magnesium nitrate hexahydrate	$Mg(NO_3)_2·6H_2O$	13446−18−9	A0460734	Thermo Scientific	98.9
aluminum chloride hexahydrate	$AlCl_3·6H_2O$	7784−13−6	R12J001	Thermo Scientific	99.5
calcium chloride dihydrate	$CaCl_2·2H_2O$	10035−04−8	240755	Fisher Bioreagents	99

structure remains limited. As noted in the literature, the lack of reliable thermophysical property data represents one of the main challenges in replacing conventional solvents with DES. Moreover, DES are often far from ideal mixtures, exhibiting complex hydrogen-bonding networks. Therefore, rigorous and systematic characterization of thermophysical and interfacial properties is essential to properly describe DES behavior and support their rational design and selection. To address this gap, the present work focuses on the measurement and analysis of several key properties of representative DES systems. Specifically, viscosity, density, speed of sound, surface tension, and contact angle were determined for DES based on choline chloride and glycerol (ChCl:Gly) at a molar ratio of 1:2, combined with $AlCl_3·6H_2O$, $MgCl_2·6H_2O$, $Mg(NO_3)_2·6H_2O$, and $CaCl_2·2H_2O$. These properties are selected due to their high relevance to both fundamental thermodynamics and practical applications.

Viscosity, density, and surface tension are key physicochemical parameters that strongly influence solvent performance in a wide range of processes.[13] Viscosity governs fluid flow, pumping requirements, mixing efficiency, heat, and mass transfer; many DES exhibit relatively high viscosities, which can hinder their practical use at scale and have been identified as a bottleneck for the industrial implementation of DES-based processes.[14] Density data are equally important for equipment design and separation operations, as they determine fluid buoyancy, hydrostatic pressure, phase behavior, and volumetric flow characteristics; accurate knowledge of density is frequently required in feasibility studies and detailed process design because it directly influences material balances, phase equilibrium calculations, and the sizing of reactors, pumps, and separators for a given DES-based system.[15] Moreover, the density of DES can vary substantially with composition and temperature, further underscoring the need for reliable experimental data to support practical applications.

Surface tension governs interfacial phenomena such as droplet formation, capillarity, and wetting, and reflects the cohesive interactions at the liquid surface. It is defined as the energy required to create a unit area of new surface or, equivalently, as the force acting along a unit length of the liquid interface.[16] DES often exhibit higher surface tension than conventional molecular solvents.[17] This elevated surface tension can significantly influence solvent−solid interactions and interfacial processes relevant to applications such as extraction, coating, and biomass pretreatment.

The speed of sound is an important thermodynamic property that provides access to key derived quantities such as compressibility, cohesive energy density, and equation of state parameters, thereby offering indirect insight into intermolecular interactions and liquid structure.[18,19] In complex, nonideal systems such as DES, variations in the speed of sound reflect changes in molecular packing and hydrogen-bonding strength, making this property particularly informative. Several thermophysical properties relevant to process design and optimization, including isentropic and isothermal compressibility, heat capacity, and thermal conductivity, can be estimated from speed-of-sound data. This is especially significant for DESs, which are designer solvents for which comprehensive thermophysical property data sets are often unavailable.[20,21]

Choline chloride-based DES are the most widely studied systems due to their low cost, availability, and compositional versatility. A commonly studied example is the ChCl:Gly molar ratio 1:2 mixture (Glyceline), for which density and viscosity have been extensively characterized over broad temperature ranges, showing well-defined temperature dependencies associated with changes in molecular packing and hydrogen-bonding interactions.[22,23] Building on this established binary system, the incorporation of a third component, such as hydrated metal salts, leads to ternary deep eutectic solvents (TDES) with modified melting behavior and transport properties compared to their binary counterparts.[24] Despite their increasing relevance, systematic studies reporting multiple thermophysical and interfacial properties, such as density, viscosity, surface tension, contact angle, and speed of sound, under consistent experimental conditions remain scarce. However, systematic comparisons between binary ChCl systems and multicomponent DES remain limited, particularly when both bulk and interfacial properties are evaluated under consistent conditions. In this work, we present a comprehensive experimental investigation of the thermophysical and interfacial properties of choline chloride/glycerol/metal salt hydrated DES systems. Density, viscosity, surface tension, contact angle, and speed of sound were measured over the temperature range of 293.15 to 343.15 K at atmospheric pressure for DES containing hydrated salts of $AlCl_3·6H_2O$, $MgCl_2·6H_2O$, $Mg(NO_3)_2·6H_2O$, and $CaCl_2·2H_2O$ at varying metal salt concentrations.

2. EXPERIMENTAL SECTION

2.1. Samples

Substances are obtained from Sigma-Aldrich. The purity of choline chloride (ChCl), glycerol (Gly), aluminum chloride hexahydrate ($AlCl_3·6H_2O$), magnesium chloride hexahydrate ($MgCl_2·6H_2O$), calcium chloride dihydrate ($CaCl_2·2H_2O$), and magnesium nitrate hexahydrate ($Mg(NO_3)_2·6H_2O$) is (99, 99.5, 99, 98.9, 99.5, and 99) mass fraction, respectively. Table 1 shows the specifications of the samples.

2.2. DES Preparation

Prior to DES preparation, Glycerol is kept over activated 4 Å molecular sieves for 7 days to remove excess water. DES are synthesized as follows: First, ChCl is kept in an oven for 24 h at a temperature of 90 °C to be free of moisture. After that, the ChCl is kept under vacuum at an absolute pressure of approximately 33.6 kPa for 12 h to eliminate the remaining water. The ChCl and the HBDs are mixed in a specific molar ratio (shown in Table 2) at 80 °C and

Downloaded from pubs.acs.org/jceaax/article-pdf/71/7/2914/6510469/acs.jced.6c00151.pdf by UNIV DE BURGOS user on 07 September 2026

https://doi.org/10.1021/acs.jced.6c00151
J. Chem. Eng. Data 2026, 71, 2914−2931

Table 2. DES Considered in This Work

DES	HAD	HBA	HBA	notation DES	molar ratio	MW
M1	choline chloride	glycerol	aluminum chloride hexahydrate	ChCl:Gly:$AlCl_3{\cdot}6H_2O$	1:2:0.1	112.24
M2	choline chloride	glycerol	aluminum chloride hexahydrate	ChCl:Gly:$AlCl_3{\cdot}6H_2O$	1:2:0.13	113.48
M3	choline chloride	glycerol	aluminum chloride hexahydrate	ChCl:Gly:$AlCl_3{\cdot}6H_2O$	1:2:0.2	116.28
M4	choline chloride	glycerol	aluminum chloride hexahydrate	ChCl:Gly:$AlCl_3{\cdot}6H_2O$	1:2:0.25	118.20
M5	choline chloride	glycerol	aluminum chloride hexahydrate	ChCl:Gly:$AlCl_3{\cdot}6H_2O$	1:2:0.28	119.33
M6	choline chloride	glycerol	aluminum chloride hexahydrate	ChCl:Gly:$AlCl_3{\cdot}6H_2O$	1:2:0.3	120.07
M7	choline chloride	glycerol	aluminum chloride hexahydrate	ChCl:Gly:$AlCl_3{\cdot}6H_2O$	1:2:0.35	121.88
M8	choline chloride	glycerol	magnesium chloride hexahydrate	ChCl:Gly:$MgCl_2{\cdot}6H_2O$	1:2:0.1	111.01
M9	choline chloride	glycerol	magnesium chloride hexahydrate	ChCl:Gly:$MgCl_2{\cdot}6H_2O$	1:2:0.13	111.90
M10	choline chloride	glycerol	magnesium chloride hexahydrate	ChCl:Gly:$MgCl_2{\cdot}6H_2O$	1:2:0.2	113.90
M11	choline chloride	glycerol	magnesium chloride hexahydrate	ChCl:Gly:$MgCl_2{\cdot}6H_2O$	1:2:0.25	115.27
M12	choline chloride	glycerol	magnesium chloride hexahydrate	ChCl:Gly:$MgCl_2{\cdot}6H_2O$	1:2:0.28	116.08
M13	choline chloride	glycerol	magnesium chloride hexahydrate	ChCl:Gly:$MgCl_2{\cdot}6H_2O$	1:2:0.3	116.61
M14	choline chloride	glycerol	magnesium chloride hexahydrate	ChCl:Gly:$MgCl_2{\cdot}6H_2O$	1:2:0.35	117.90
M15	choline chloride	glycerol	calcium chloride dihydrate	ChCl:Gly:$CaCl_2{\cdot}2H_2O$	1:2:0.1	109.20
M16	choline chloride	glycerol	calcium chloride dihydrate	ChCl:Gly:$CaCl_2{\cdot}2H_2O$	1:2:0.13	109.56
M17	choline chloride	glycerol	calcium chloride dihydrate	ChCl:Gly:$CaCl_2{\cdot}2H_2O$	1:2:0.2	110.38
M18	choline chloride	glycerol	calcium chloride dihydrate	ChCl:Gly:$CaCl_2{\cdot}2H_2O$	1:2:0.25	110.94
M19	choline chloride	glycerol	calcium chloride dihydrate	ChCl:Gly:$CaCl_2{\cdot}2H_2O$	1:2:0.3	111.49
M20	choline chloride	glycerol	calcium chloride dihydrate	ChCl:Gly:$CaCl_2{\cdot}2H_2O$	1:2:0.35	112.02
M21	choline chloride	glycerol	magnesium nitrate hexahydrate	ChCl:Gly:$Mg(NO_3)_2{\cdot}6H_2O$	1:2:0.1	112.73
M22	choline chloride	glycerol	magnesium nitrate hexahydrate	ChCl:Gly:$Mg(NO_3)_2{\cdot}6H_2O$	1:2:0.15	115.01
M23	choline chloride	glycerol	magnesium nitrate hexahydrate	ChCl:Gly:$Mg(NO_3)_2{\cdot}6H_2O$	1:2:0.2	117.22
M24	choline chloride	glycerol	magnesium nitrate hexahydrate	ChCl:Gly:$Mg(NO_3)_2{\cdot}6H_2O$	1:2:0.25	119.36
M25	choline chloride	glycerol	magnesium nitrate hexahydrate	ChCl:Gly:$Mg(NO_3)_2{\cdot}6H_2O$	1:2:0.30	121.43
M26	choline chloride	glycerol	magnesium nitrate hexahydrate	ChCl:Gly:$Mg(NO_3)_2{\cdot}6H_2O$	1:2:0.35	123.45

with continuous agitation at 300 rpm. This procedure is stopped when a homogeneous, transparent mixture is formed; generally, this occurs after three hours. The DES is placed in a vacuum desiccator at 20−25 in of Hg. DES are prepared gravimetrically, measuring the masses of each component with an analytical balance (Ohaus model AS120S) of 0.1 mg accuracy. The estimated standard uncertainty[25] of the mole fraction is less than 0.001. Before measurements, mixtures are kept in close airtight containers to avoid evaporation. Water content is controlled through the use of hydrated salts and consistent sample handling during preparation and measurements. All samples are prepared under the same conditions to ensure reproducibility. These DES are type II and III according to the classification of Smith et al.[26]

The molar ratios selected for the DES systems are not arbitrary but are guided by preliminary findings from ongoing delignification studies. These compositions demonstrated an effective lignin removal performance.

2.3. Apparatuses and Procedures

2.3.1. Density and Speed of Sound. Densities and speeds of sound of the DES are measured using a vibrating tube densimeter (Anton Paar DMS 5000) with two independent cells. This instrument operates based on the vibrating U-tube principle to measure the density. The sample is introduced into a U-shaped tube that oscillates at its natural resonance frequency, which is directly related to the mass of the fluid inside the tube and thus to its density. By comparing the measured resonance frequency with calibration standards (ultrapure water and air), the density of the sample is determined. Density and temperature reproducibility from the manufacturer are 1×10^{-6} g·cm^{-3} and 0.001 K, respectively. We have used the consideration given by Chirico et al.[27] to estimate a standard relative density uncertainty of 0.001. For the $CaCl_2$ system at n = 0.2, a slightly higher relative uncertainty of 0.0025 is assigned due to minor variability during sample preparation. A Pt-100 thermometer with a standard uncertainty of 0.01 K is built in the densimeter. In the speed-of-sound cell, its determination is achieved through integrated ultrasonic transducers that emit and detect acoustic pulses traveling through the fluid. The transit time of the sound wave over a known path length is used to calculate the speed of sound. The standard uncertainty of the speed-of-sound measurements is 2 m s^{-1}.

2.3.2. Viscosity. Viscosity measurements are carried out using a rotational rheometer (Anton Paar MCR 502). The rheometer determines viscosity by measuring the torque required to impose a controlled deformation on the sample. A cone−plate geometry with a 49.98 mm diameter, an 0.997°-angle, and a 0.101 mm gap is employed to measure the viscosity. All measurements are performed after instrument calibration following the manufacturer's recommendations. The viscosity of the rotational rheometer is verified using certified Newtonian silicone oil standards with ISO 17025 traceable viscosity values. Care was taken during sample loading to avoid air bubbles and to ensure correct gap filling. All viscosity measurements are performed at a constant shear rate of 50 s^{-1}. The relative uncertainty associated with the viscosity measurements is estimated to be within 6%, depending on the sample and measurement conditions.

2.3.3. Surface Tension and Contact Angle. Surface tension and contact angle measurements are carried out to characterize the interfacial behavior of the DES. All measurements are performed at 298.15 K and an atmospheric pressure of 0.1 MPa using the same optical setup, consisting of a high-resolution camera (Edmund FMVU-03MTM-CS, Point Gray Research) and associated image analysis software. The optical system is calibrated prior to measurements using ultrapure water as a reference fluid with a well-established surface tension at 298.15 K. The measured values are verified against literature data to ensure accuracy. Optical calibration is performed by adjusting the scaling parameters based on the known needle diameter, ensuring accurate droplet profile analysis and fitting to the Young−Laplace equation. Surface tension is determined by using the pendant drop method. Pendant droplets are formed at the tip of a needle and imaged under controlled illumination conditions, with the droplet occupying approximately 50% or more of the vertical field of view to ensure accurate fitting. Surface tension values are obtained by fitting the droplet shape to the Young−Laplace equation. Three independent pendant droplets are analyzed for each DES

Downloaded from pubs.acs.org/jceaax/article-pdf/71/7/2914/6510469/acs.jced.6c00151.pdf by UNIV DE BURGOS user on 07 September 2026

https://doi.org/10.1021/acs.jced.6c00151
J. Chem. Eng. Data 2026, 71, 2914−2931

Table 3. Experimental and Calculated Densities (from Equations 4−7), ρ, at Temperature T and Pressure p = 0.1 MPa for the DES

DES	T/K	ρ^{exp}/g cm^{-3}	ρ^{cal}/g cm^{-3}	DES	ρ^{exp}/g cm^{-3}	ρ^{cal}/g cm^{-3}	DES	ρ^{exp}/g cm^{-3}	ρ^{cal}/g cm^{-3}	DES	ρ^{exp}/g cm^{-3}	ρ^{cal}/g cm^{-3}
M1	293.15	1.2168	1.2168	**M8**	1.2076	1.2074	**M15**	1.2122	1.2121	**M21**	1.2132	1.2131
	298.15	1.2140	1.2140		1.2049	1.2047		1.2095	1.2094		1.2104	1.2104
	303.15	1.2112	1.2112		1.2022	1.2020		1.2068	1.2067		1.2076	1.2076
	308.15	1.2084	1.2084		1.1995	1.1994		1.2041	1.2040		1.2048	1.2048
	313.15	1.2055	1.2055		1.1968	1.1967		1.2014	1.2013		1.2020	1.2020
	318.15	1.2028	1.2027		1.1941	1.1940		1.1986	1.1986		1.1992	1.1992
	323.15	1.1999	1.1999		1.1913	1.1914		1.1959	1.1959		1.1965	1.1965
	328.15	1.1971	1.1971		1.1886	1.1887		1.1932	1.1932		1.1937	1.1937
	333.15	1.1942	1.1942		1.1859	1.1860		1.1905	1.1905		1.1909	1.1909
	338.15	1.1914	1.1914		1.1831	1.1834		1.1877	1.1878		1.1881	1.1881
	343.15	1.1885	1.1886		1.1804	1.1807		1.1850	1.1852		1.1853	1.1853
M2	293.15	1.2227	1.2227	**M9**	1.2132	1.2134	**M16**	1.2166	1.2165	**M22**	1.2249	1.2250
	298.15	1.2199	1.2199		1.2109	1.2107		1.2139	1.2138		1.2221	1.2222
	303.15	1.2171	1.2171		1.2082	1.2080		1.2112	1.2111		1.2194	1.2194
	308.15	1.2142	1.2142		1.2055	1.2054		1.2085	1.2085		1.2166	1.2166
	313.15	1.2114	1.2114		1.2028	1.2027		1.2058	1.2058		1.2138	1.2138
	318.15	1.2086	1.2086		1.2001	1.2000		1.2031	1.2031		1.2110	1.2110
	323.15	1.2058	1.2058		1.1974	1.1974		1.2004	1.2004		1.2082	1.2082
	328.15	1.2030	1.2029		1.1947	1.1947		1.1976	1.1977		1.2054	1.2054
	333.15	1.2001	1.2001		1.1920	1.1920		1.1949	1.1950		1.2026	1.2026
	338.15	1.1973	1.1973		1.1892	1.1894		1.1922	1.1923		1.1998	1.1999
	343.15	1.1944	1.1945		1.1865	1.1867		1.1895	1.1896		1.1970	1.1971
M3	293.15	1.2397	1.2398	**M10**	1.2251	1.2250	**M17**	1.2282	1.2282	**M23**	1.2355	1.2354
	298.15	1.2369	1.2369		1.2224	1.2224		1.2255	1.2255		1.2327	1.2326
	303.15	1.2341	1.2341		1.2197	1.2197		1.2228	1.2228		1.2299	1.2298
	308.15	1.2313	1.2313		1.2170	1.2170		1.2201	1.2201		1.2271	1.2270
	313.15	1.2284	1.2284		1.2143	1.2144		1.2174	1.2174		1.2243	1.2242
	318.15	1.2256	1.2256		1.2117	1.2117		1.2148	1.2147		1.2215	1.2214
	323.15	1.2228	1.2228		1.2090	1.2091		1.2121	1.2120		1.2187	1.2186
	328.15	1.2200	1.2200		1.2063	1.2064		1.2094	1.2093		1.2159	1.2158
	333.15	1.2171	1.2171		1.2037	1.2037		1.2066	1.2066		1.2131	1.2130
	338.15	1.2143	1.2143		1.2010	1.2011		1.2039	1.2040		1.2103	1.2102
	343.15	1.2114	1.2115		1.1983	1.1984		1.2012	1.2013		1.2075	1.2074
M4	293.15	1.2493	1.2493	**M11**	1.2324	1.2323	**M18**	1.2415	1.2416	**M24**	1.2449	1.2449
	298.15	1.2466	1.2465		1.2298	1.2296		1.2389	1.2389		1.2420	1.2421
	303.15	1.2438	1.2437		1.2271	1.2269		1.2362	1.2362		1.2392	1.2393
	308.15	1.2410	1.2409		1.2245	1.2243		1.2335	1.2335		1.2364	1.2365
	313.15	1.2381	1.2380		1.2217	1.2216		1.2308	1.2308		1.2336	1.2337
	318.15	1.2353	1.2352		1.2191	1.2189		1.2281	1.2281		1.2308	1.2309
	323.15	1.2325	1.2324		1.2165	1.2163		1.2255	1.2254		1.2280	1.2281
	328.15	1.2297	1.2296		1.2138	1.2136		1.2228	1.2228		1.2252	1.2253
	333.15	1.2268	1.2267		1.2112	1.2109		1.2201	1.2201		1.2224	1.2225
	338.15	1.2240	1.2239		1.2085	1.2083		1.2174	1.2174		1.2195	1.2196
	343.15	1.2211	1.2211		1.2059	1.2056		1.2147	1.2147		1.2167	1.2168
M5	293.15	1.2559	1.2561	**M12**	1.2362	1.2366	**M19**	1.2502	1.2503	**M25**	1.2540	1.2539
	298.15	1.2532	1.2533		1.2336	1.2339		1.2475	1.2476		1.2511	1.2511
	303.15	1.2504	1.2505		1.2309	1.2313		1.2449	1.2449		1.2483	1.2483
	308.15	1.2476	1.2477		1.2282	1.2286		1.2422	1.2422		1.2455	1.2455
	313.15	1.2448	1.2448		1.2255	1.2259		1.2395	1.2395		1.2427	1.2427
	318.15	1.2419	1.2420		1.2229	1.2233		1.2369	1.2369		1.2399	1.2398
	323.15	1.2390	1.2392		1.2203	1.2206		1.2341	1.2342		1.2371	1.2370
	328.15	1.2362	1.2363		1.2176	1.2179		1.2315	1.2315		1.2342	1.2342
	333.15	1.2334	1.2335		1.2150	1.2153		1.2288	1.2288		1.2314	1.2314
	338.15	1.2305	1.2307		1.2123	1.2126		1.2262	1.2261		1.2286	1.2286
	343.15	1.2277	1.2279		1.2097	1.2099		1.2235	1.2234		1.2258	1.2257
M6	293.15	1.2611	1.2610	**M13**	1.2396	1.2395	**M20**	1.2603	1.2604	**M26**	1.2624	1.2624
	298.15	1.2583	1.2582		1.2369	1.2368		1.2576	1.2577		1.2595	1.2595
	303.15	1.2555	1.2553		1.2343	1.2342		1.2550	1.2550		1.2567	1.2567
	308.15	1.2526	1.2525		1.2316	1.2315		1.2523	1.2523		1.2539	1.2539
	313.15	1.2498	1.2497		1.2290	1.2288		1.2496	1.2496		1.2511	1.2511

Downloaded from pubs.acs.org/jceaax/article-pdf/71/7/2914/6510546 9/acs.jced.6c00151.pdf by UNIV DE BURGOS user on 07 September 2026

https://doi.org/10.1021/acs.jced.6c00151
J. Chem. Eng. Data 2026, 71, 2914−2931

Table 3. continued

DES	T/K	ρ^{exp}/g cm^{-3}	ρ^{cal}/g cm^{-3}	DES	ρ^{exp}/g cm^{-3}	ρ^{cal}/g cm^{-3}	DES	ρ^{exp}/g cm^{-3}	ρ^{cal}/g cm^{-3}	DES	ρ^{exp}/g cm^{-3}	ρ^{cal}/g cm^{-3}
	318.15	1.2470	1.2469		1.2263	1.2262		1.2469	1.2469		1.2482	1.2482
	323.15	1.2441	1.2440		1.2237	1.2235		1.2442	1.2442		1.2454	1.2454
	328.15	1.2413	1.2412		1.2211	1.2208		1.2416	1.2415		1.2426	1.2426
	333.15	1.2384	1.2384		1.2185	1.2182		1.2389	1.2389		1.2397	1.2397
	338.15	1.2356	1.2356		1.2158	1.2155		1.2363	1.2362		1.2369	1.2369
	343.15	1.2327	1.2327		1.2132	1.2128		1.2336	1.2335		1.2341	1.2341
M7	293.15	1.2695	1.2695	**M14**	1.2461	1.2463						
	298.15	1.2666	1.2667		1.2434	1.2436						
	303.15	1.2638	1.2638		1.2408	1.2409						
	308.15	1.2610	1.2610		1.2382	1.2383						
	313.15	1.2582	1.2582		1.2355	1.2356						
	318.15	1.2554	1.2553		1.2328	1.2329						
	323.15	1.2525	1.2525		1.2303	1.2303						
	328.15	1.2497	1.2497		1.2277	1.2276						
	333.15	1.2468	1.2469		1.2251	1.2249						
	338.15	1.2440	1.2440		1.2225	1.2223						
	343.15	1.2412	1.2412		1.2199	1.2196						

composition, and the reported values correspond to the average of these measurements.

Contact angle measurements were conducted using the sessile drop method to evaluate the wetting behavior of the DES on solid substrates. A small droplet of the DES was deposited onto the surface of the substrate, and the static contact angle at the three-phase contact line was determined by fitting the droplet profile using the Young equation. Measurements were performed on glass, copper, and stainless steel 316 substrates. Three independent measurements were carried out for each DES combination, and the reported values represent the average contact angle.

The experimental uncertainty is estimated as the standard deviation of replicate measurements. The uncertainty for surface tension is 1.29 mN·m^{-1}. For contact angle measurements, the uncertainties are 3.85°, 2.78°, and 2.83° for glass, stainless steel 316, and copper, respectively.

3. RESULTS

3.1. Density

The density of DES varies systematically with composition and temperature. Variations in density reflect changes in molecular packing and hydrogen-bonding interactions between the hydrogen-bond donor and acceptor. Also, accurate density data are essential for process design, equipment sizing, and modeling of mass and heat transfer in applications where DESs are employed. In this work, we have measured the liquid density of the DES from 293.15 to 343.15 K. Table 3 shows the experimental density values for the DESs.

We have correlated the densities for each DES using

$$\rho = a + bT \tag{1}$$

where a and b are parameters obtained from the experimental data. Table 4 shows the values of the parameters together with the standard deviation of the residuals defined as

$$\mathrm{SDR} = \sqrt{\frac{\sum_{i=1}^{\mathrm{npts}} (J^{\mathrm{exp}} - J^{\mathrm{calc}})^2}{\mathrm{npts} - \mathrm{nparm}}} \tag{2}$$

The superscripts exp and calc stand for experimental and calculated, respectively, and npts and nparms are the number of experimental points and number of parameters. The variable J stands for the experimental property (density, speed of sound, etc.).

Table 4. Parameters for Equation 1

DES	a	b	SDR
M1	1.3822	-5.642×10^{-4}	4.288×10^{-5}
M2	1.3884	-5.650×10^{-4}	3.061×10^{-5}
M3	1.4056	-5.658×10^{-4}	2.254×10^{-5}
M4	1.4147	-5.640×10^{-4}	4.872×10^{-5}
M5	1.4222	-5.667×10^{-4}	5.116×10^{-5}
M6	1.4276	-5.678×10^{-4}	2.402×10^{-5}
M7	1.4352	-5.654×10^{-4}	2.367×10^{-5}
M8	1.3673	-5.447×10^{-4}	1.176×10^{-5}
M9	1.3712	-5.379×10^{-4}	9.999×10^{-5}
M10	1.3817	-5.346×10^{-4}	2.100×10^{-5}
M11	1.3883	-5.317×10^{-4}	2.931×10^{-5}
M12	1.3917	-5.304×10^{-4}	2.846×10^{-5}
M13	1.3941	-5.273×10^{-4}	3.662×10^{-5}
M14	1.3996	-5.240×10^{-4}	4.131×10^{-5}
M15	1.3745	-5.442×10^{-4}	1.811×10^{-5}
M16	1.3786	-5.431×10^{-4}	2.903×10^{-5}
M17	1.3887	-5.384×10^{-4}	2.924×10^{-5}
M18	1.4013	-5.357×10^{-4}	1.792×10^{-5}
M19	1.4095	-5.343×10^{-4}	2.189×10^{-5}
M20	1.4196	-5.345×10^{-4}	1.945×10^{-5}
M21	1.3766	-5.575×10^{-4}	9.084×10^{-6}
M22	1.3887	-5.586×10^{-4}	9.306×10^{-6}
M23	1.3997	-5.601×10^{-4}	1.249×10^{-5}
M24	1.4098	-5.628×10^{-4}	1.192×10^{-5}
M25	1.4192	-5.637×10^{-4}	1.704×10^{-5}
M26	1.4281	-5.654×10^{-4}	1.878×10^{-5}

Regression analyses are performed using SAS software (SAS Institute Inc., Cary, NC, USA), which seeks the best model from a databank of terms. It begins with the one-variable model that yields the highest R-square and then adds the variable that produces the greatest improvement. For each model size, the regression systematically evaluates all possible variable substitutions, making the switch that maximizes R-square and repeating the process until no further improvement is possible. The following equation is selected because, within the set of 63 k_i-terms, it includes temperature- and composition-dependent contributions capable of representing the liquid density of a DES with both accuracy and model simplicity

Downloaded from pubs.acs.org/jceaax/article-pdf/71/7/2914/6510469/acs.jced.6c00151.pdf by UNIV DE BURGOS user on 07 September 2026

https://doi.org/10.1021/acs.jced.6c00151
J. Chem. Eng. Data 2026, 71, 2914−2931

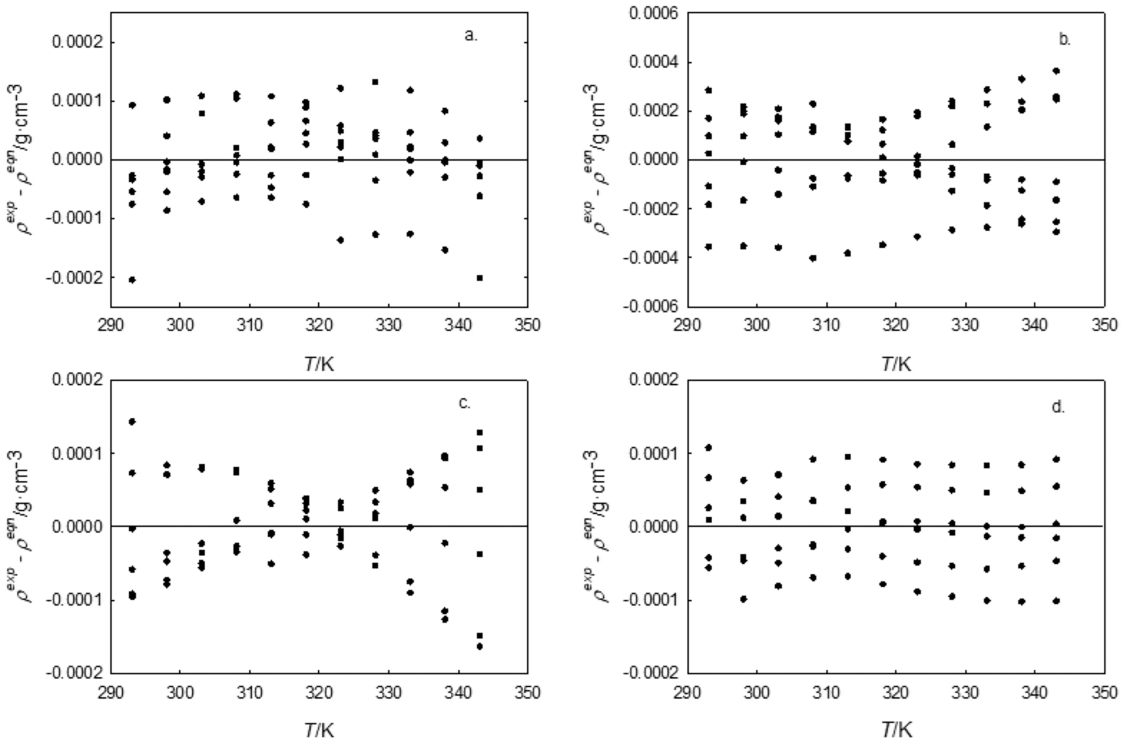

Figure 1. Density deviations from eqs 4−7 as a function of temperature. Panels correspond to $AlCl_3{\cdot}6H_2O$ (a), $MgCl_2{\cdot}6H_2O$ (b), $CaCl_2{\cdot}6H_2O$ (c), and $Mg(NO_3)_2{\cdot}6H_2O$ (d). Density deviations from eq 4 (a), AAPD = 0.006%; eq 5 (b), AAPD = 0.016%; eq 6 (c), AAPD = 0.006%; and eq 7 (d), AAPD = 0.004%.

$$\rho = \sum_{i=1}^{7} k_{ij} n^{(i-1)/2} \sum_{j=1}^{9} T^{(i-1)/4} \tag{3}$$

where k_{ij} are the selecting parameters, n is the number of moles of the metallic salt, and T is the temperature in K. The final selected equations are

$$\rho = 1.35894 + 11.07807n^{0.5} - 127.135n + 578.1744n^{1.5} - 1295.79n^2 + 1434.549n^{2.5} - 628.096n^3 - 5.656 \times 10^{-4}T \tag{4}$$

$$\rho = 1.34832 + 0.7334n^{0.5} - 9.40112n + 47.44256n^{1.5} - 113.13688n^2 + 130.81794n^{2.5} - 59.10843n^3 - 5.32296 \times 10^{-4}T \tag{5}$$

$$\rho = 1.35044 - 15.7953n^{0.5} + 184.5144n - 845.772n^{1.5} + 1909.155n^2 - 2121.971n^{2.5} + 930.030n^3 - 5.3837 \times 10^{-4}T \tag{6}$$

$$\rho = 1.35487 - 0.56605n^{0.5} - 3.916 \times 10^{-5}n + 6.18047n^{1.5} - 17.82094n^2 + 22.61769n^{2.5} - 10.82897n^3 - 5.5232 \times 10^{-4}T \tag{7}$$

Equations 4−7 are for aluminum chloride, magnesium chloride, calcium chloride, and magnesium nitrate, respectively. Table 3 shows the experimental density data with the calculated density using the above equations. The maximum density deviation observed is 0.0004 for the DES composed of $MgCl_2{\cdot}6H_2O$ (M12) at n = 0.28. Equations 4−7 predict correctly the experimental density values of glyceline from Perez-Duran et al.[28] within an average absolute percentage deviation of 0.018%.

Although the proposed correlations are empirical, the fitted parameters reflect the underlying physicochemical behavior. The models reproduce the experimental data while capturing meaningful trends associated with DES structural organization, consistent with Halder et al.[29] While not fully predictive, they provide reliable interpolation within the studied range and a basis for future semipredictive approaches.

The density of the investigated DESs increases with increasing metal salt content and decreases approximately linearly with temperature across all systems (M1−M26). This behavior reflects systematic changes in intermolecular interactions and packing efficiency within the liquid structure. In the ChCl−glycerol system,[2] a chloride hydrogen-bond network gives a moderately structured liquid with available free volume. The addition of hydrated metal salts perturbs this network while introducing stronger ion−dipole and coordination interactions with glycerol, which collectively promote more efficient molecular packing and a reduction in free volume.

At comparable compositions, density increases follow the trend $Al^{3+} > Mg^{2+} \approx Ca^{2+} > Mg(NO_3)_2$. This trend is consistent with differences in cation charge density and ion−solvent interaction strength. In particular, Al^{3+}, due to its high charge density and strong Lewis acidity, is expected to exhibit stronger coordination interactions with oxygen-containing species; therefore, there are more compact local solvation environments. In contrast, Mg^{2+} and Ca^{2+} exhibit comparatively weaker interactions and more loosely hydration structures, resulting in less compact structures. Nitrate-based systems display similar but slightly reduced density increases,

Downloaded from pubs.acs.org/jceaax/article-pdf/71/7/2914/6510469/acs.jced.6c00151.pdf by UNIV DE BURGOS user on 07 September 2026

https://doi.org/10.1021/acs.jced.6c00151
J. Chem. Eng. Data 2026, 71, 2914−2931

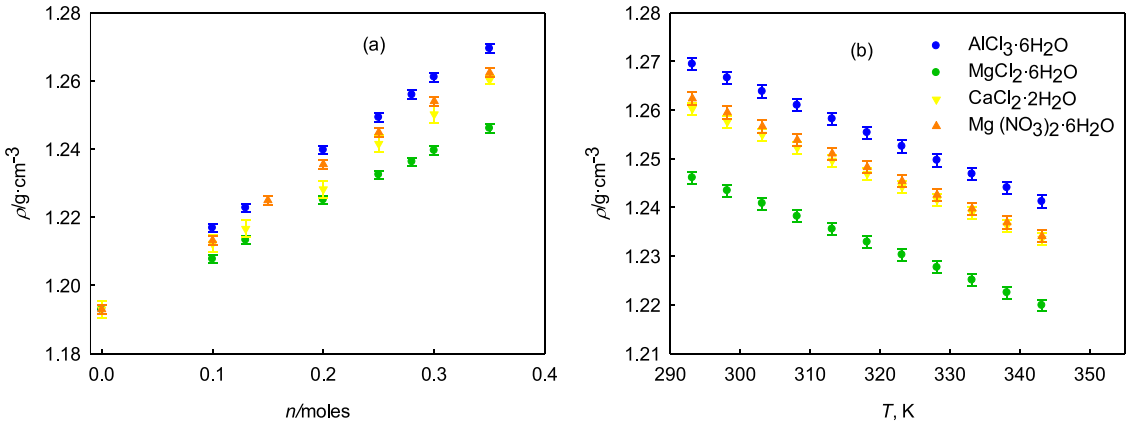

Figure 2. (a) Experimental density as a function of moles of hydrated metal salts for ternary DES systems at 293.15 K. (b) Temperature dependence of density for ternary DES systems at a constant salt number of moles of $n = 0.35$ within the range of 293.15 to 343.15 K. Error bars are equal to 2σ.

indicating that anion identity and packing effects also contribute to the overall structural response.[30]

Hydration effects further influence these trends. Strongly bound hydration shells associated with Al^{3+} may enhance local structuring and packing efficiency, whereas more dynamic hydration environments around Mg^{2+} and Ca^{2+} lead to weaker structuring effects. Water introduced via hydrated salts may also participate in hydrogen bonding, potentially acting as a bridge within the existing network and modifying local organization.[31] Overall, density variations arise from a combined effect of ion−solvent coordination, hydration, and hydrogen-bond network rearrangement (Figure 1).

As observed in Figure 2a, the density increases linearly with increasing salt concentration across all systems, which suggests a consistent integration of the hydrated salts into the ChCl:Gly hydrogen-bonded network. However, the $AlCl_3.6H_2O$ system (M1−M7) exhibits the most pronounced density enhancement. From a fundamental thermodynamic perspective, this is attributed to the high charge density of the trivalent Al^{3+} cation compared to the divalent Mg^{2+}/Ca^{2+} species. The ion induces a superior electro restriction effect, effectively pulling the hydroxyl groups of glycerol molecules and the chloride anions into a more compact coordination shell. This results in higher packing efficiency and a more compact liquid structure with reduced free volume. In Figure 2a, the density of glyceline[28] ($n = 0$) at 293.15 of 1.1929 g·cm^{-3} is the baseline, indicating that the incorporation of hydrated metal salts leads to a systematic increase in density across all systems. This increase shows the impact of salt addition on the structural organization of the DES matrix.

The temperature dependence depicted in Figure 2b shows a strictly linear decrease in density ($\partial\rho/\partial T < 0$), consistent with the thermal expansion of the supramolecular network. Aluminum-based systems maintain higher density values even at higher temperatures, suggesting that the coordination between the Al^{3+} centers and the hydroxyl groups of glycerol creates a more robust, thermally resistant structure. This hierarchical ordering ($Al^{3+} > Mg^{2+} > Ca^{2+}$) underscores the ability to tune the macroscopic density of the DES by selecting metal salts with specific coordination geometries and ionic strengths, a critical factor for the rational design of solvents for industrial separation processes.

3.2. Speed of Sound

The speed of sound is a thermophysical property that provides information about the compressibility, intermolecular interactions, and structural organization of liquid systems. In the DES with metal salts, the speed of sound is influenced by the ionic character and the formation of structured hydrogen-bonding and coordination networks. We have measured the speed of sound under the same conditions as the density, and they are shown in Table 5. Our measurements have been correlated using a quadratic polynomial in temperature

$$u = a_u + b_u T + c_u T^2 \tag{8}$$

where a_u, b_u, and c_u are parameters obtained from the data. Table 6 shows the parameters with the standard deviation from the fit.

We have expressed the speed of sound as a function of the temperature and the number of moles of the metallic salt

$$u = 48107 - 673.256T^{0.25} + (-161621 + 56896T^{0.25} - 1042.66T^{0.75})n + (4290905 - 2313629T^{0.25} + 320716T^{0.5} - 10.02T^{1.75})n^{1.5} \tag{9}$$

$$u = 3372.24 - 78.7614T^{0.5} + (-50717 + 17794T^{0.25} - 322.768T^{0.75})n + (2009983 - 1090928T^{0.25} + 152257T^{0.5} - 4.9376T^{1.75})n^{1.5} \tag{10}$$

$$u = 2368.18 - 0.01668T^{1.75} + 106.280T^{0.25}n^{0.5} + 1073478n - 584149T^{0.25}n + 81498T^{0.5}n - 2.62293T^{1.75}n + 6124.56n^{1.5} - 238.165T^{0.5}n^2 \tag{11}$$

$$u = 3365.293 - 78.3712T^{0.5} - 228.594n^{0.5} + 52.28412T^{0.25}n^{0.5} + (2996185 - 1651594T^{0.25} + 234094T^{0.5} - 8.19464T^{1.75})n^3 \tag{12}$$

Equations 9−12 correspond to DES with a metallic salt of aluminum chloride, magnesium chloride, calcium chloride, and magnesium nitrate. Figure 3 shows the deviations from eqs 9−12. In Figures 1 and 3, we have included the average absolute percentage deviation defined as

https://doi.org/10.1021/acs.jced.6c00151
J. Chem. Eng. Data 2026, 71, 2914−2931

Downloaded from pubs.acs.org/jceaax/article-pdf/71/7/2914/6510469/acs.jced.6c00151.pdf by UNIV DE BURGOS user on 07 September 2026

Table 5. Experimental and Calculated Speed of Sound (from Equations 9−12), u, at Temperature T and Pressure p = 0.1 MPa for the DES

DES	T/K	u^{exp}/m s^{-1}	u^{cal}/m s^{-1}	DES	u^{exp}/m s^{-1}	u^{cal}/m s^{-1}	DES	u^{exp}/m s^{-1}	u^{cal}/m s^{-1}	DES	u^{exp}/m s^{-1}	u^{cal}/m s^{-1}
M1	293.15	2040.8	2036.6	**M8**	2036.1	2035.7	**M15**	2029.1	2024.5	**M21**	2019.4	2019.6
	298.15	2027.5	2025.0		2024.2	2024.3		2016.9	2013.8		2008.0	2008.5
	303.15	2015.1	2013.5		2012.8	2013.0		2005.2	2003.2		1997.0	1997.5
	308.15	2003.3	2002.1		2001.8	2001.9		1993.9	1992.7		1986.3	1986.5
	313.15	1991.9	1990.9		1990.9	1990.9		1982.9	1982.4		1975.6	1975.7
	318.15	1980.6	1979.7		1980.1	1980.0		1972.0	1972.2		1965.0	1964.9
	323.15	1969.5	1968.8		1969.4	1969.2		1961.3	1962.0		1954.5	1954.3
	328.15	1958.5	1957.9		1958.7	1958.5		1950.7	1952.0		1944.0	1943.7
	333.15	1947.5	1947.2		1948.1	1947.9		1940.1	1942.1		1933.4	1933.2
	338.15	1936.6	1936.7		1937.4	1937.5		1929.6	1932.4		1922.8	1922.8
	343.15	1925.6	1926.3		1926.6	1927.2		1919.3	1922.7		1912.3	1912.4
M2	293.15	2045.0	2043.2	**M9**	2041.7	2040.5	**M16**	2029.5	2027.9	**M22**	2019.5	2018.9
	298.15	2031.4	2030.8		2029.1	2028.9		2017.6	2016.6		2007.8	2007.8
	303.15	2018.6	2018.6		2016.6	2017.4		2006.2	2005.5		1996.7	1996.7
	308.15	2006.5	2006.7		2005.3	2006.1		1995.2	1994.5		1985.8	1985.9
	313.15	1994.9	1995.0		1994.4	1994.9		1984.4	1983.6		1975.1	1975.1
	318.15	1983.6	1983.6		1983.6	1983.9		1973.7	1972.9		1964.5	1964.4
	323.15	1972.8	1972.4		1972.9	1973.1		1963.2	1962.3		1954.0	1953.8
	328.15	1961.3	1961.4		1962.2	1962.4		1952.8	1951.9		1943.4	1943.3
	333.15	1950.3	1950.7		1951.6	1951.9		1942.5	1941.6		1932.9	1932.8
	338.15	1939.4	1940.3		1941.0	1941.6		1932.1	1931.5		1922.3	1922.4
	343.15	1928.5	1930.1		1930.4	1931.4		1922.0	1921.5		1911.9	1912.1
M3	293.15	2061.8	2062.2	**M10**	2055.5	2053.5	**M17**	2037.8	2044.1	**M23**	2019.5	2018.4
	298.15	2043.9	2047.1		2041.4	2040.8		2025.4	2031.2		2007.5	2007.2
	303.15	2028.6	2032.5		2028.7	2028.5		2012.7	2018.6		1996.3	1996.1
	308.15	2015.0	2018.5		2017.0	2016.5		2001.3	2006.3		1985.4	1985.3
	313.15	2002.5	2005.2		2005.7	2004.8		1990.3	1994.3		1974.7	1974.5
	318.15	1990.6	1992.5		1994.7	1993.5		1979.5	1982.6		1964.1	1963.9
	323.15	1979.0	1980.5		1983.9	1982.4		1969.0	1971.2		1953.6	1953.4
	328.15	1967.8	1969.1		1973.1	1971.7		1958.6	1960.2		1943.1	1942.9
	333.15	1956.7	1958.3		1962.4	1961.2		1948.4	1949.5		1932.6	1932.5
	338.15	1945.8	1948.2		1951.8	1951.1		1938.2	1939.1		1922.1	1922.2
	343.15	1935.0	1938.8		1941.0	1941.3		1928.2	1929.0		1911.7	1911.8
M4	293.15	2071.0	2078.6	**M11**	2064.4	2063.9	**M18**	2052.1	2048.1	**M24**	2017.6	2018.2
	298.15	2053.4	2060.7		2049.9	2050.3		2035.5	2033.3		2006.0	2006.8
	303.15	2037.7	2043.7		2035.7	2037.1		2021.0	2019.0		1994.9	1995.6
	308.15	2024.0	2027.8		2023.4	2024.5		2007.9	2005.3		1984.2	1984.7
	313.15	2011.3	2012.9		2011.4	2012.2		1995.8	1992.1		1973.7	1974.0
	318.15	1999.8	1999.0		2000.3	2000.5		1984.3	1979.6		1963.3	1963.5
	323.15	1987.7	1986.1		1989.4	1989.1		1973.2	1967.5		1953.0	1953.0
	328.15	1976.3	1974.3		1978.7	1978.3		1962.5	1956.1		1942.6	1942.6
	333.15	1965.8	1963.4		1968.0	1967.8		1952.0	1945.3		1932.2	1932.3
	338.15	1954.0	1953.6		1957.4	1957.9		1941.7	1935.0		1921.8	1921.9
	343.15	1943.1	1944.9		1946.9	1948.3		1931.7	1925.3		1911.4	1911.5
M5	293.15	2094.9	2089.4	**M12**	2067.8	2070.5	**M19**	2071.5	2064.9	**M25**	2018.7	2018.3
	298.15	2071.2	2069.5		2053.6	2056.2		2050.3	2046.4		2006.6	2006.5
	303.15	2050.9	2051.0		2039.9	2042.5		2031.0	2029.9		1995.3	1995.2
	308.15	2033.9	2033.7		2027.8	2029.4		2017.2	2015.1		1984.4	1984.2
	313.15	2019.3	2017.7		2016.5	2016.8		2003.2	2001.8		1973.7	1973.6
	318.15	2006.1	2002.9		2005.5	2004.7		1989.8	1989.5		1963.3	1963.1
	323.15	1993.8	1989.5		1994.6	1993.2		1977.4	1978.1		1952.9	1952.7
	328.15	1981.9	1977.3		1983.8	1982.2		1965.8	1967.3		1942.2	1942.4
	333.15	1970.4	1966.4		1973.1	1971.8		1954.9	1956.8		1932.1	1932.1
	338.15	1959.2	1956.8		1962.6	1961.9		1944.3	1946.3		1921.6	1921.7
	343.15	1948.0	1948.5		1951.9	1952.6		1934.2	1935.8		1911.3	1911.2
M6	293.15	2107.9	2096.9	**M13**	2078.3	2075.1	**M20**	2074.7	2076.0	**M26**	2018.6	2018.6
	298.15	2078.6	2075.7		2060.2	2060.4		2052.6	2055.7		2006.2	2006.4
	303.15	2056.1	2056.0		2044.9	2046.2		2034.1	2036.8		1994.8	1994.8
	308.15	2037.7	2037.7		2031.4	2032.7		2018.5	2019.5		1983.9	1983.8
	313.15	2022.2	2020.9		2019.2	2019.9		2004.7	2003.7		1973.3	1973.1

Downloaded from pubs.acs.org/jceaax/article-pdf/71/7/2914/6510546 9/acs.jced.6c00151.pdf by UNIV DE BURGOS user on 07 September 2026

https://doi.org/10.1021/acs.jced.6c00151
J. Chem. Eng. Data 2026, 71, 2914−2931

Table 5. continued

DES	T/K	u^{exp}/m s^{-1}	u^{cal}/m s^{-1}	DES	u^{exp}/m s^{-1}	u^{cal}/m s^{-1}	DES	u^{exp}/m s^{-1}	u^{cal}/m s^{-1}	DES	u^{exp}/m s^{-1}	u^{cal}/m s^{-1}
	318.15	2008.7	2005.5		2007.7	2007.6		1992.3	1989.3		1962.7	1962.7
	323.15	1996.5	1991.7		1996.6	1995.9		1980.6	1976.5		1952.5	1952.4
	328.15	1983.9	1979.2		1985.7	1984.9		1969.5	1965.3		1942.2	1942.2
	333.15	1972.4	1968.3		1975.0	1974.5		1959.0	1955.6		1931.8	1931.9
	338.15	1961.4	1958.8		1964.3	1964.6		1948.7	1947.5		1921.3	1921.5
	343.15	1950.9	1950.8		1953.9	1955.4		1938.9	1940.9		1911.0	1910.8
M7	293.15	2122.1	2117.1	**M14**	2091.5	2087.1						
	298.15	2089.1	2092.1		2071.0	2071.0						
	303.15	2063.2	2069.1		2054.2	2055.8						
	308.15	2042.5	2048.1		2039.8	2041.3						
	313.15	2025.1	2029.1		2027.0	2027.7						
	318.15	2010.2	2012.1		2015.1	2014.9						
	323.15	1996.8	1997.1		2003.9	2002.8						
	328.15	1984.4	1984.0		1992.9	1991.6						
	333.15	1972.6	1972.9		1982.1	1981.1						
	338.15	1961.3	1963.8		1971.5	1971.4						
	343.15	1950.5	1956.7		1960.7	1962.5						

Table 6. Parameters Used in Equation 8

DES	a_u	b_u	c_u	SDR
M1	3127.33	−4.929	4.162×10^{-3}	0.45
M2	3214.51	−5.433	4.917×10^{-3}	0.54
M3	4049.92	−10.476	1.258×10^{-2}	1.24
M4	4024.56	−10.239	1.217×10^{-2}	1.30
M5	5403.98	−18.539	2.470×10^{-2}	2.24
M6	6302.57	−24.020	3.307×10^{-2}	3.23
M7	7258.52	−29.751	4.165×10^{-2}	3.65
M8	2872.40	−3.434	1.977×10^{-3}	0.27
M9	3092.39	−4.769	4.033×10^{-3}	0.51
M10	3286.25	−5.867	5.680×10^{-3}	0.70
M11	3621.29	−7.879	8.748×10^{-3}	0.80
M12	3463.43	−6.888	7.243×10^{-3}	0.80
M13	4143.12	−11.010	1.351×10^{-2}	1.42
M14	4593.33	−13.692	1.756×10^{-2}	1.88
M15	3046.99	−4.470	3.537×10^{-3}	0.25
M16	2993.92	−4.175	3.149×10^{-3}	0.23
M17	3275.15	−5.844	5.677×10^{-3}	0.41
M18	4014.34	−10.205	1.214×10^{-2}	0.96
M19	5920.73	−21.501	2.889×10^{-2}	2.24
M20	5272.55	−17.684	2.331×10^{-2}	1.85
M21	2772.77	−2.947	1.281×10^{-3}	0.19
M22	2832.05	−3.313	1.842×10^{-3}	0.24
M23	2877.32	−3.601	2.296×10^{-3}	0.31
M24	2822.09	−3.290	1.856×10^{-3}	0.31
M25	2930.32	−3.950	2.860×10^{-3}	0.37
M26	2951.74	−4.088	3.079×10^{-3}	0.44

$$\mathrm{AAPD} = \frac{1}{N}\sum_{i}\left|\frac{J_i^{exp} - J_i^{calc}}{J_i^{exp}}\right| \times 100 \quad (13)$$

Equations 9−12 extrapolate to predict the speed of sound of glyceline[28] $n = 0$ within an average absolute percentage deviation of 0.025%.

The speed of sound provides complementary insight into the adiabatic compressibility and the effective stiffness of the liquid structure. In all systems, the speed of sound decreases with an increase in temperature, reflecting enhanced molecular mobility and reduced structural rigidity.

In contrast, increasing metal salt concentration leads to higher sound velocities, indicating reduced compressibility and a more cohesive liquid structure driven by stronger intermolecular interactions. Among the studied systems, Al^{3+}-containing DESs consistently exhibit the highest speed-of-sound values, in agreement with stronger ion−dipole interactions and enhanced coordination between Al^{3+}, glycerol, and coordinated water.

At a fixed temperature, chloride-based systems generally display higher sound velocities than nitrate-based systems, suggesting stronger intermolecular cohesion and lower compressibility. The effect is most pronounced in Al^{3+} systems, which show a marked increase in sound velocity compared to the parent ChCl:Gly DES.[2] This behavior is attributed to the strong Lewis acidity and high charge density of Al^{3+}, which promotes strong coordination with oxygen donor species and increases the effective connectivity of the liquid structure. These interactions reduce compressibility and lead to an apparent increase in the effective stiffness of the system, as reflected in the higher sound velocities.[32]

By contrast, nitrate-containing systems exhibit lower or only slightly altered sound velocities despite higher densities. This decoupling between density and compressibility suggests that NO_3^- acts as a hydrogen-bond network modifier, weakening directional interactions within the ChCl:Gly matrix and limiting the formation of more strongly interconnected structures.[30]

The acoustic profiles presented in Figure 4a,4b provide a fundamental diagnostic of the structural rigidity and isentropic compressibility (κ) of the ternary DES networks. Again, as in the density, we have included the speed of sound of the binary ChCl:Gly (1:2)[28] system ($n = 0$) in Figure 4a. This value (2023.7 m·s^{-1} at 293.15 K) is for the speed of sound when hydrated metal salts are included. In most cases, this leads to a systematic increase in acoustic velocity, indicating reduced compressibility and enhanced structural rigidity of the DES matrix, except for $Mg(NO_3)_2{\cdot}6H_2O$.

As dictated by the Newton−Laplace relationship, the monotonic increase in acoustic velocity with salt addition indicates that the hydrated metal cations effectively stiffen the hydrogen-bonded matrix by filling interstitial cavities and reducing intermolecular free volume. At low to moderate

Downloaded from pubs.acs.org/jceaax/article-pdf/71/7/2914/6510469/acs.jced.6c00151.pdf by UNIV DE BURGOS user on 07 September 2026

https://doi.org/10.1021/acs.jced.6c00151
J. Chem. Eng. Data 2026, 71, 2914−2931

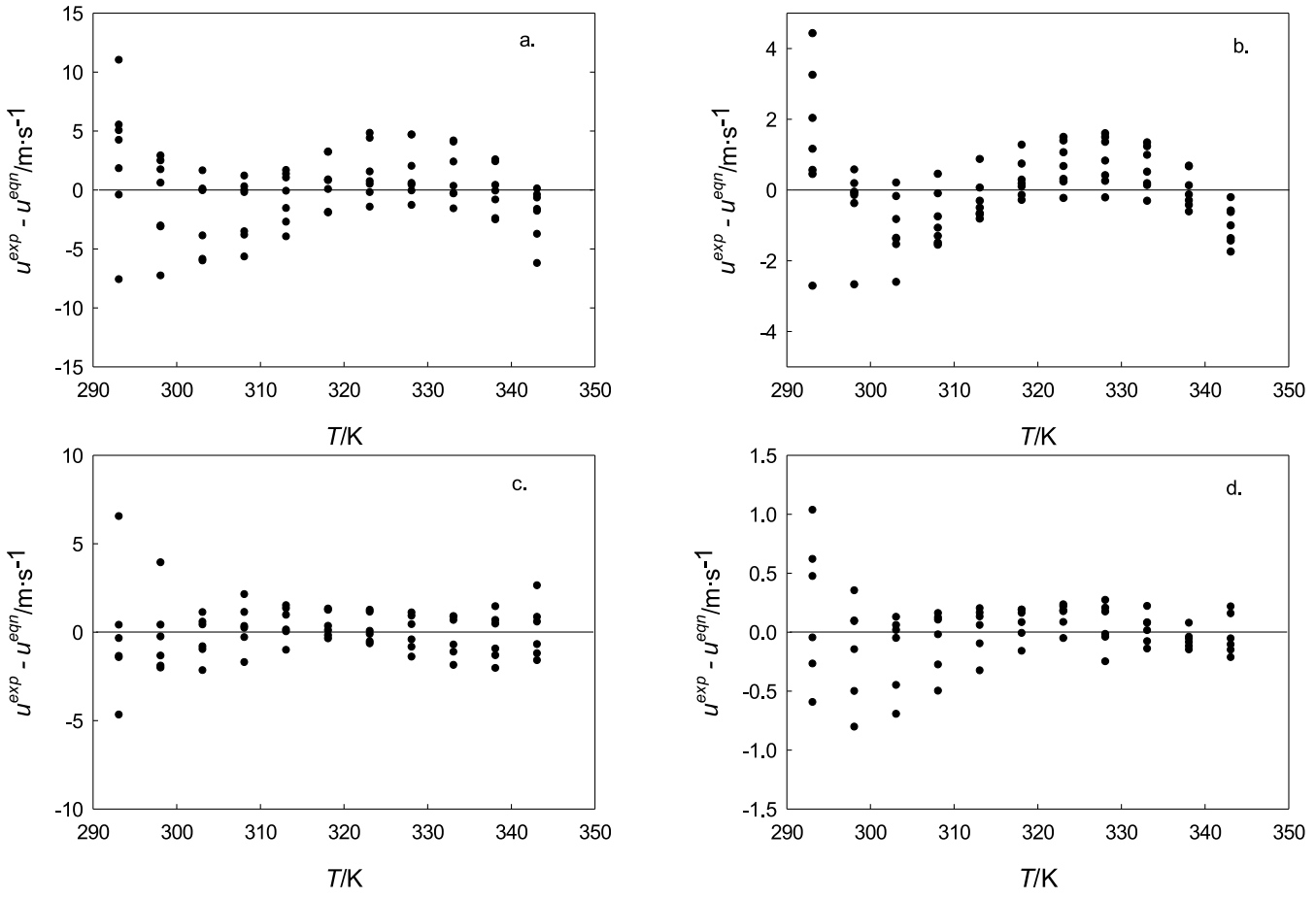

Figure 3. Speed-of-sound deviations from eqs 9−12 as a function of temperature. Panels correspond to $AlCl_3{\cdot}6H_2O$ (a), $MgCl_2{\cdot}6H_2O$ (b), $CaCl_2{\cdot}6H_2O$ (c), and $Mg(NO_3)_2{\cdot}6H_2O$ (d). Speed-of-sound deviations from eq 9 (a), AAPD = 0.12%; eq 10 (b), AAPD = 0.04%; eq 11 (c), AAPD = 0.05%; and eq 12 (d), AAPD = 0.008%.

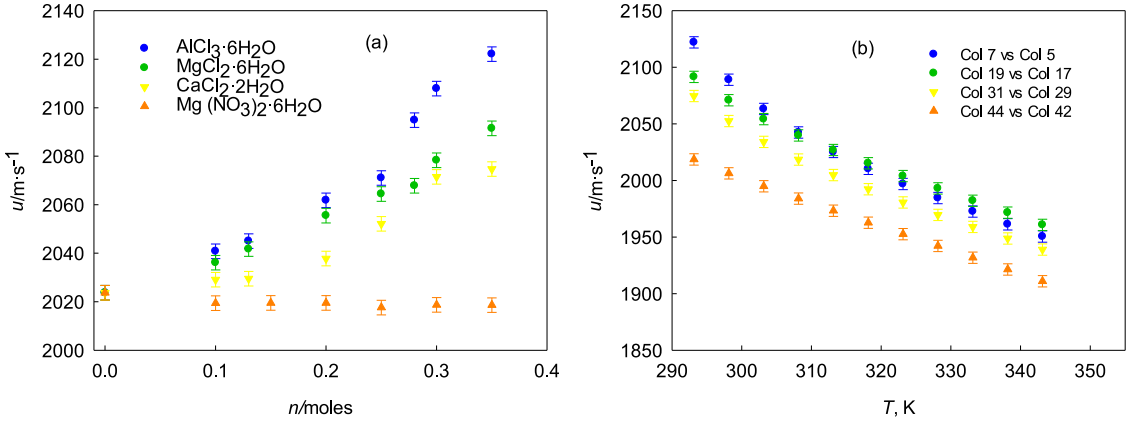

Figure 4. (a) Experimental speed of sound as a function of the molar fraction of hydrated metal salts for ternary DES systems at 293.15 K. (b) Temperature dependence of speed of sound for ternary DES systems at a constant salt number of moles of n = 0.35 within the range of 293.15 to 343.15 K. Error bars are equal to 2σ.

concentrations (n = 0.1−0.2), the $AlCl_3.6H_2O$ system exhibits the most pronounced acoustic stiffening, as the Al^{3+} cation induces immense electrostriction, tightly organizing glycerol and chloride ions into a rigid secondary coordination sphere.

Furthermore, the linear decrease in acoustic velocity with an increase in temperature (Figure 4b) reflects classical thermal softening, where enhanced kinetic energy expands the supramolecular lattice and weakens cohesive hydrogen bonding across all systems. The molecular geometry of the incorporated ions heavily dictates the acoustic wave propagation. For instance, despite containing the structuring Mg^{2+} cation, the $Mg(NO_3)_2{\cdot}6H_2O$ system yields the lowest acoustic velocities; the bulky, planar nitrate anions disrupt optimal molecular packing, acting as structural softeners that offset cationic electrostriction.

Notably, convergence and crossover behavior occur between the $AlCl_3$ and $MgCl_2$ systems as the molar fraction approaches the highly congested limit of n = 0.35. At this concentration,

Downloaded from pubs.acs.org/jceaax/article-pdf/71/7/2914/6510546/acs.jced.6c00151.pdf by UNIV DE BURGOS user on 07 September 2026

https://doi.org/10.1021/acs.jced.6c00151
J. Chem. Eng. Data 2026, 71, 2914−2931

Table 7. Experimental and Calculated Viscosities (from Equation 13), η, at Temperature T and Pressure p = 0.1 MPa for the DES

DES	T/K	η^{exp}/mPa·s	η^{cal}/mPa·s	DES	T/K	η^{exp}/mPa·s	η^{cal}/mPa·s	DES	T/K	η^{exp}/mPa·s	η^{cal}/mPa·s	DES	T/K	η^{exp}/mPa·s	η^{cal}/mPa·s
M1	293.09	969.9	971.0	**M8**	293.09	656.3	657.1	**M15**	293.09	596.6	596.7	**M21**	293.15	312.5	312.7
	298.06	670.6	668.2		298.06	471.0	469.7		298.06	418.5	418.3		298.15	222.3	221.7
	303.03	472.0	471.4		303.02	344.0	342.7		303.02	300.9	300.7		303.15	160.8	161.3
	307.99	338.7	340.2		307.99	254.4	254.7		307.99	221.0	221.2		308.15	120.4	120.0
	312.97	248.8	250.4		312.97	191.1	192.5		312.97	166.0	166.0		313.15	90.6	91.1
	317.93	187.0	188.0		317.93	146.5	147.8		317.92	127.1	127.1		318.15	70.1	70.4
	322.90	143.3	143.4		322.90	114.3	115.1		322.90	98.7	98.8		323.15	55.5	55.3
	327.88	111.4	111.1		327.88	90.6	90.8		327.88	77.8	78.1		328.15	44.1	44.1
	332.86	87.8	87.3		332.85	72.9	72.5		332.86	62.5	62.5		333.15	35.5	35.7
	337.83	70.3	69.5		337.83	59.4	58.5		337.83	50.8	50.7		338.15	29.4	29.2
	342.96	57.1	55.7		342.96	49.3	47.5		342.96	41.8	41.4		343.15	24.6	24.2
M2	293.10	1283.7	1284.0	**M9**	293.10	877.0	877.4	**M16**	293.09	677.8	679.3	**M22**	293.15	323.0	323.2
	298.06	876.9	876.4		298.06	615.5	614.3		298.06	475.4	469.4		298.15	228.4	227.8
	303.03	613.8	613.3		303.03	440.6	440.7		303.02	328.6	334.6		303.15	164.1	164.7
	307.99	439.2	439.0		307.99	322.8	323.2		307.99	244.3	245.0		308.15	121.9	121.8
	312.97	319.9	320.5		312.96	241.4	241.6		312.96	184.7	183.8		313.15	92.1	92.0
	317.93	237.8	238.7		317.93	183.8	184.0		317.93	142.0	140.9		318.15	70.7	70.8
	322.90	180.0	180.6		322.90	142.1	142.4		322.90	110.8	110.1		323.15	55.4	55.3
	327.87	138.4	138.9		327.88	111.5	111.8		327.88	87.7	87.4		328.15	43.8	43.9
	332.85	108.2	108.3		332.85	89.0	89.0		332.85	70.5	70.6		333.15	35.2	35.4
	337.82	86.2	85.6		337.82	72.1	71.8		337.83	57.3	57.7		338.15	28.9	28.8
	342.96	69.8	68.0		342.96	59.1	58.2		342.96	47.4	47.6		343.15	24.1	23.8
M3	293.09	2611.8	2614.0	**M10**	293.09	1560.0	1560.8	**M17**	293.09	1335.9	1332.3	**M23**	293.15	323.9	324.3
	298.06	1740.5	1734.9		298.06	1072.9	1071.2		298.05	897.8	907.4		298.15	231.4	229.9
	303.03	1179.8	1180.0		303.02	753.1	753.2		303.02	639.2	637.8		303.15	165.5	167.1
	307.99	818.1	821.3		307.99	541.5	541.2		307.99	465.6	461.0		308.15	124.3	124.2
	312.97	581.7	583.2		312.96	396.0	396.7		312.96	345.4	341.5		313.15	94.6	94.1
	317.93	421.1	422.5		317.93	294.9	296.3		317.92	260.6	258.7		318.15	72.4	72.6
	322.90	309.7	311.2		322.90	223.7	224.8		322.90	199.8	199.8		323.15	57.0	57.0
	327.88	232.5	232.9		327.88	172.8	173.3		327.87	155.8	157.0		328.15	45.3	45.4
	332.86	178.2	176.9		332.86	135.6	135.4		332.85	123.4	125.4		333.15	36.5	36.6
	337.83	138.5	136.3		337.83	108.1	107.2		337.83	99.1	101.6		338.15	30.0	29.9
	342.96	109.3	105.5		342.96	87.7	85.3		342.96	80.7	82.9		343.15	25.0	24.7
M4	293.03	4656.5	4657.2	**M11**	293.09	2140.5	2141.9	**M18**	293.13	2416.5	2418.3	**M24**	293.15	352.1	351.1
	298.00	3020.8	3018.9		298.06	1445.9	1443.0		298.09	1648.6	1645.4		298.15	242.2	245.2
	302.97	2008.2	2008.8		303.02	998.9	997.6		303.05	1145.5	1143.6		303.15	177.4	176.3
	307.94	1368.7	1368.9		307.99	704.5	705.9		308.02	811.5	810.4		308.15	131.9	130.1
	312.92	952.4	952.8		312.96	507.9	510.1		312.98	581.0	584.7		313.15	98.4	98.3
	317.87	676.9	678.0		317.92	374.0	376.0		317.95	424.4	429.0		318.15	75.6	75.8
	322.85	489.4	490.4		322.90	281.1	281.9		322.93	316.7	319.5		323.15	59.7	59.5
	327.83	360.6	360.8		327.87	214.9	214.8		327.90	240.7	241.3		328.15	47.1	47.5
	332.81	270.2	269.7		332.85	167.0	166.1		332.87	186.5	184.8		333.15	38.2	38.5
	337.79	205.6	204.5		337.82	131.8	130.3		337.85	147.1	143.3		338.15	31.3	31.6

https://doi.org/10.1021/acs.jced.6c00151
J. Chem. Eng. Data 2026, 71, 2914−2931

Downloaded from pubs.acs.org/jceaax/article-pdf/71/7/2914/6510546 9/acs.jced.6c00151.pdf by UNIV DE BURGOS user on 07 September 2026

Table 7. continued

DES	T/K	η^{exp}/mPa·s	η^{cal}/mPa·s	DES	T/K	η^{exp}/mPa·s	η^{cal}/mPa·s	DES	T/K	η^{exp}/mPa·s	η^{cal}/mPa·s	DES	T/K	η^{exp}/mPa·s	η^{cal}/mPa·s
	342.77	159.0	157.2		342.96	105.7	102.7		342.91	117.0	111.9		343.15	26.0	26.3
M5	293.03	6583.8	6578.2	**M12**	293.10	2827.2	2828.2	**M19**	293.09	3665.7	3662.7	**M25**	293.15	357.6	357.4
	298.00	4196.2	4216.3		298.06	1877.2	1874.3		298.06	2402.0	2410.6		298.15	251.7	253.2
	302.97	2784.4	2770.3		303.03	1275.8	1276.5		303.03	1632.0	1631.3		303.15	186.2	183.7
	307.94	1871.2	1862.3		307.99	890.2	891.0		308.00	1139.0	1131.9		308.15	135.7	136.1
	312.92	1279.1	1277.9		312.96	634.7	635.7		312.97	807.2	803.6		313.15	102.2	102.8
	317.87	890.7	895.4		317.93	462.7	463.2		317.93	582.5	582.8		318.15	78.3	79.1
	322.85	632.2	637.6		322.90	343.1	343.5		322.90	428.4	430.3		323.15	61.7	61.8
	327.83	458.9	461.6		327.87	258.6	259.2		327.88	321.2	323.3		328.15	48.9	49.0
	332.81	338.7	339.5		332.85	198.6	198.6		332.86	244.0	246.7		333.15	39.3	39.3
	337.79	253.5	253.3		337.82	155.3	154.4		337.83	189.7	191.1		338.15	32.2	32.0
	342.77	192.8	191.4		342.96	123.5	120.7		342.96	149.3	148.9		343.15	26.9	26.3
M6	293.03	8237.2	8237.0	**M13**	293.03	3227.4	3229.2	**M20**	293.03	6315.3	6308.9	**M26**	293.15	396.6	396.2
	298.00	5206.5	5204.0		298.00	2117.4	2113.5		298.00	4027.6	4045.6		298.15	275.1	276.3
	302.97	3369.8	3379.8		302.97	1423.6	1422.1		302.97	2673.4	2672.9		303.15	198.5	198.2
	307.94	2254.5	2251.0		307.95	978.2	980.8		307.94	1828.5	1814.2		308.15	146.2	145.7
	312.92	1539.7	1533.0		312.92	688.1	692.1		312.92	1270.2	1260.9		313.15	110.4	109.6
	317.88	1071.1	1068.3		317.88	498.1	499.2		317.87	898.9	897.9		318.15	83.4	84.0
	322.85	757.3	757.9		322.85	366.7	366.5		322.85	648.6	651.1		323.15	65.8	65.6
	327.83	545.7	547.3		327.83	273.9	273.7		327.83	476.0	481.0		328.15	51.9	52.1
	332.81	399.8	401.8		332.81	208.4	207.7		332.81	356.1	361.4		333.15	41.6	41.9
	337.79	297.4	299.7		337.79	162.0	159.9		337.78	271.1	275.9		338.15	34.0	34.2
	342.77	224.1	226.6		342.77	128.2	124.8		342.76	210.5	213.6		343.15	28.4	28.3
M7	293.03	13182.4	13179.7	**M14**	293.03	5063.1	5063.2								
	298.00	8203.8	8209.3		298.00	3266.6	3263.6								
	302.97	5251.8	5258.6		302.97	2159.7	2167.4								
	307.95	3464.1	3454.4		307.94	1480.6	1478.7								
	312.92	2331.3	2323.2		312.92	1037.9	1033.0								
	317.88	1603.0	1598.8		317.87	742.0	739.3								
	322.85	1119.4	1120.7		322.85	538.5	538.8								
	327.83	788.1	799.8		327.83	397.3	399.9								
	332.81	576.3	580.5		332.81	299.7	301.9								
	337.79	427.4	428.1		337.79	230.6	231.5								
	342.77	320.8	320.3		342.77	180.5	180.0								

https://doi.org/10.1021/acs.jced.6c00151
J. Chem. Eng. Data 2026, 71, 2914−2931

Downloaded from pubs.acs.org/joeaax/article-pdf/71/7/2914/6510546 9/acs.jced.6c00151.pdf by UNIV DE BURGOS user on 07 September 2026

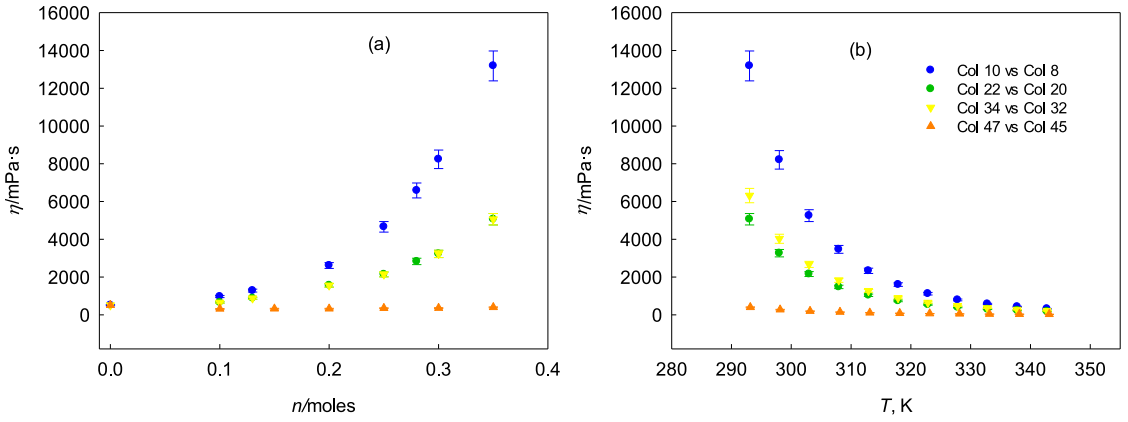

Figure 5. (a) Experimental viscosity as a function of the number of moles of hydrated metal salts for ternary DES systems at 293.15 K. (b) Temperature dependence of viscosity for ternary DES systems at n = 0.35 within the range of 293.15 to 343.15 K. Error bars are equal to 2σ.

the rigid, highly charged Al^{3+} complexes suffer from the exhaustion of thermodynamic free volume, whereas the more conformationally flexible Mg^{2+} system maintains efficient secondary packing, allowing its acoustic velocity to ultimately match and slightly surpass that of the sterically jammed aluminum system.

Also, the speed-of-sound profiles closely mirror the density trends, exhibiting identical hierarchical dependencies on the metal cations (Al^{3+} > Mg^{2+} > Ca^{2+}) and salt concentration, which demonstrates a direct macroscopic correlation where the electrostrictive densification of the supramolecular matrix fundamentally dictates its enhanced acoustic stiffness.

3.3. Viscosity

Viscosity is an important physicochemical property, as it plays a key role in industrial processes, such as mass transport, diffusion, and fluid handling. Therefore, the viscosity of DES is essential for solvent design and optimization. The viscosity of DES based on glyceline is relatively high due to the extensive hydrogen-bonding network formed between hydrogen-bond donor and acceptor species. The incorporation of metal salts, such as those considered in this work, modifies the viscosity by strengthening ionic interactions and increasing the structural organization within the solvent. As a result, the addition of metal salts to glyceline leads to a noticeable increase in viscosity, which depends on both temperature and salt concentration. We have measured the viscosity of the DES in the temperature range from 298.15 to 343.15 K. Table 7 shows the experimental viscosity values for the DESs.

The viscosity of all systems decreases strongly with an increase in temperature and increases significantly with metal salt concentration. This behavior reflects thermally activated structural relaxation combined with enhanced intermolecular interactions at higher ionic strengths.

At low salt content, the rheological behavior is primarily governed by the hydrogen-bond network of the ChCl−glycerol DES.[2] Upon addition of metal salts, stronger ion−dipole interactions and coordination between metal cations and glycerol hydroxyl groups lead to the formation of transient ionic−coordination clusters. These dynamic associations hinder molecular mobility and increase resistance to flow.

Among the studied systems, Al^{3+}-containing DESs exhibit the highest viscosities, consistent with stronger Lewis acidity and higher charge density, which enhance coordination interactions with available donor sites. Mg^{2+} systems generally show higher viscosities than Ca^{2+} systems, which may be attributed to differences in hydration structure and ion−solvent interaction strength, influencing the lifetime and stability of transient aggregates.[33]

Water introduced through hydrated salts further affects viscosity by modifying hydrogen-bonding interactions and competing with glycerol for coordination sites. At the same time, water may facilitate additional bridging interactions within the liquid structure. The overall viscosity behavior therefore reflects a dynamic balance between ion−solvent coordination, hydrogen-bond network rearrangement, and disruption effects introduced by hydration.

Figure 5 shows the composition dependence of the viscosity at 293.15 for the DES and the temperature dependence at n = 0.35. This figure shows a nonlinear increase in viscosity with salt content (Figure 5a), which may be related to tighter molecular packing and less free space for movement as coordination interactions develop. The temperature dependence (Figure 5b) follows Arrhenius behavior. This is an indication of higher activation energy as salt concentration increases, possibly due to stronger ion−dipole interactions. The higher viscosities in Al^{3+} systems may indicate stronger or more frequent coordination, while differences between Mg^{2+} and Ca^{2+} could be linked to variations in their hydration shells and ionic size. In Figures 2, 4, and 5, the values at n = 0 (ChCl:Gly, 1:2) have been taken from Perez-Duran et al.[28]

In this work, the viscosity of each DES is represented using the Vogel−Tammann−Fulcher (VTF) equation

$$\eta = \eta_0 \exp\left(\frac{B}{T - T_0}\right) \tag{14}$$

where η_0 in mPa·s, B in K, and T_0 in K are parameters obtained from the experimental data. In eq 14, η_0 represents the limiting viscosity at high temperature, B reflects the energy barrier for viscous flow, and T_0 corresponds to the temperature at which molecular mobility would theoretically cease. Values of the parameters are in Table 8. The parameters are obtained by fitting the experimental viscosity data using a nonlinear least-squares method. The optimization is performed using the Marquardt algorithm implemented in SAS, without applying weighting factors.

3.4. Surface Tension and Contact Angle

Surface tension (γ) and contact angle (θ) values of choline chloride:glycerol:metal salt hydrated DES measured at 298.15 K are summarized in Table 9. The γ values range from

Downloaded from pubs.acs.org/jceaax/article-pdf/71/7/2914/6510469/acs.jced.6c00151.pdf by UNIV DE BURGOS user on 07 September 2026

https://doi.org/10.1021/acs.jced.6c00151
J. Chem. Eng. Data 2026, 71, 2914−2931

Table 8. Parameters of Equation 14

DES	η_0/mPa·s	B/K	T_0/K	SDR
M1	0.0198	1496.39	154.565	1.41
M2	0.0158	1606.05	151.062	0.85
M3	0.0053	2018.89	139.178	3.01
M4	0.0041	2158.05	138.204	1.20
M5	0.0012	2605.98	124.858	9.85
M6	0.0030	2305.50	137.533	4.87
M7	0.0024	2454.67	134.966	7.19
M8	0.0141	1655.44	139.038	1.23
M9	0.0364	1368.05	157.517	0.61
M10	0.0189	1633.72	148.756	1.33
M11	0.0181	1656.87	151.232	2.08
M12	0.0174	1678.41	153.235	1.62
M13	0.0114	1785.85	150.792	2.75
M14	0.0195	1697.17	156.907	3.81
M15	0.0435	1220.53	164.970	0.21
M16	0.1480	912.90	184.818	3.09
M17	0.1763	986.71	182.596	4.51
M18	0.0032	2289.49	123.829	3.60
M19	0.0195	1690.64	153.863	4.52
M20	0.0179	1761.80	155.114	9.64
M21	0.0387	1132.15	167.311	0.39
M22	0.0312	1175.71	165.990	0.34
M23	0.0326	1185.44	165.357	0.82
M24	0.0791	939.97	181.221	1.35
M25	0.0226	1306.99	157.950	1.14
M26	0.0546	1052.00	174.820	0.63

approximately 40.5 to 53.4 mN·m^{-1}, demonstrating a clear dependence on the concentration of the hydrated metal salt. Aluminum and magnesium chloride-based DES generally exhibit higher surface tensions (43−53 mN·m^{-1}), which can be attributed to stronger ionic interactions and hydrogen-bonding networks within the DES structure. In contrast, several calcium chloride-based systems display lower γ values, with values approaching 41 mN·m^{-1}, suggesting a partial weakening of cohesive interactions within the DES structure as calcium salt content increases.

DESs containing magnesium nitrate hexahydrate tend to show comparatively higher γ values than their chloride analogues, reflecting differences in anion solvation and hydration that promote a more structured interfacial region.

While variations in γ alone do not fully dictate wettability, lower surface tension values generally favor reduced contact angles. Nevertheless, the absence of a strict linear relationship between γ and θ indicates that wetting behavior arises from a balance between DES internal structure, ionic composition, and solid−liquid interfacial interactions. This tunability of surface tension through metal salt selection offers a practical way to tailor DES for applications where controlled interfacial behavior is required.

Contact angle measurements reveal a clear dependence on substrate type. Wettability is described by the contact angle (θ), where $\theta < 90°$ indicates favorable liquid−solid adhesion and spreading, while $\theta > 90°$ corresponds to reduced wettability.

As illustrated in Figure 6, distinct wetting regimes are observed depending on both the substrate and DES composition. On glass surfaces (Figure 6a−c), DESs based on choline chloride:glycerol:calcium chloride dihydrate exhibit a wide range of contact angles, ranging from highly favorable to marginally nonwetting behavior. Specifically, ChCl:Gly:$CaCl_2$·$2H_2O$ (1:2:0.35, M20) shows highly favorable wetting ($\theta \approx 39°$; Figure 6a), whereas increasing the calcium salt concentration to intermediate levels (1:2:0.2, M17) results in marginally nonwetting behavior ($\theta \approx 94°$; Figure 6c). Intermediate wetting behavior is observed for Aluminum-

Table 9. Experimental Surface Tension (γ) and Contact Angles (θ) on Glass, Stainless Steel 316, and Copper Measured at Temperature T = 298.15 K and Pressure P = 0.1 MPa for the Studied DES; Reported Values Correspond to Mean ± Standard Deviation (SD)[a]

DES	T/K	γ/mN·m^{-1}	SD	θ glass	SD	θ Steel 316	SD	θ copper	SD
M1	298.15	49.65	4.87	84.54	5.24	89.42	2.65	116.29	5.88
M3	298.15	53.40	0.29	84.19	3.34	98.59	0.71	114.57	0.91
M4	298.15	50.98	0.87	53.43	5.30	85.06	2.12	91.23	1.50
M6	298.15	44.56	0.77	61.43	1.16	88.52	3.26	90.15	1.96
M7	298.15	43.61	0.33	75.36	4.16	95.79	9.24	110.18	3.94
M8	298.15	48.04	1.87	72.78	2.16	91.01	2.74	108.53	6.83
M10	298.15	40.48	0.36	72.12	4.34	106.97	0.58	119.28	1.91
M11	298.15	52.41	0.65	71.12	1.93	109.97	3.13	114.43	6.68
M13	298.15	48.33	3.92	70.16	5.56	101.10	2.14	107.84	2.91
M14	298.15	50.69	1.06	48.83	2.61	91.91	1.13	102.73	1.43
M15	298.15	41.23	0.36	70.81	5.63	109.99	0.07	112.67	2.44
M17	298.15	41.77	2.17	93.67	7.30	112.74	2.59	117.24	2.04
M18	298.15	44.39	2.52	83.46	6.64	100.68	5.12	121.99	1.22
M19	298.15	43.79	0.43	59.40	2.24	100.74	3.79	106.01	3.99
M20	298.15	48.13	0.14	39.37	3.55	99.53	1.56	96.69	3.21
M21	298.15	51.63	0.49	81.81	1.00	97.75	2.61	117.93	1.39
M23	298.15	42.24	0.38	90.90	2.36	106.91	4.20	116.62	4.37
M24	298.15	49.80	0.54	71.10	8.23	82.19	4.73	91.27	1.63
M25	298.15	50.50	0.42	55.09	1.09	84.11	0.73	88.13	1.55
M26	298.15	52.82	3.31	67.78	3.15	92.46	2.49	93.44	0.81

[a] $\mathrm{SD} = \sqrt{\frac{\sum_{i=1}^{n}(x_i - \bar{x})^2}{n-1}}$

Downloaded from pubs.acs.org/jceaax/article-pdf/7/7/2914/6510469/acs.jced.6c00151.pdf by UNIV DE BURGOS user on 07 September 2026

https://doi.org/10.1021/acs.jced.6c00151
J. Chem. Eng. Data 2026, 71, 2914−2931

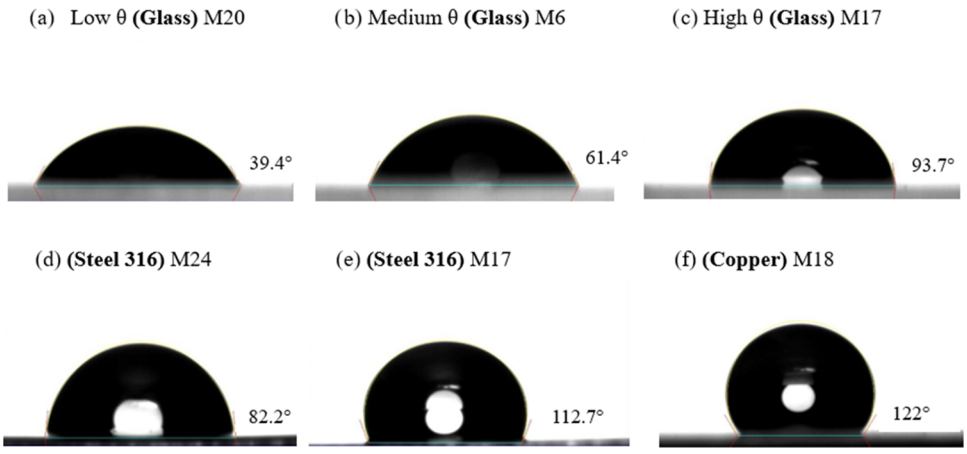

Figure 6. Representative contact angle images of selected choline chloride:glycerol:metal salt hydrated DES on glass, stainless steel 316, and copper surfaces at 298.15 K and 0.1 MPa. Panels (a–c) illustrate low, intermediate, and high wetting regimes on glass, while panels (d–f) show representative wetting behavior on stainless steel 316 and copper. DES codes and corresponding contact angle values are indicated in each panel.

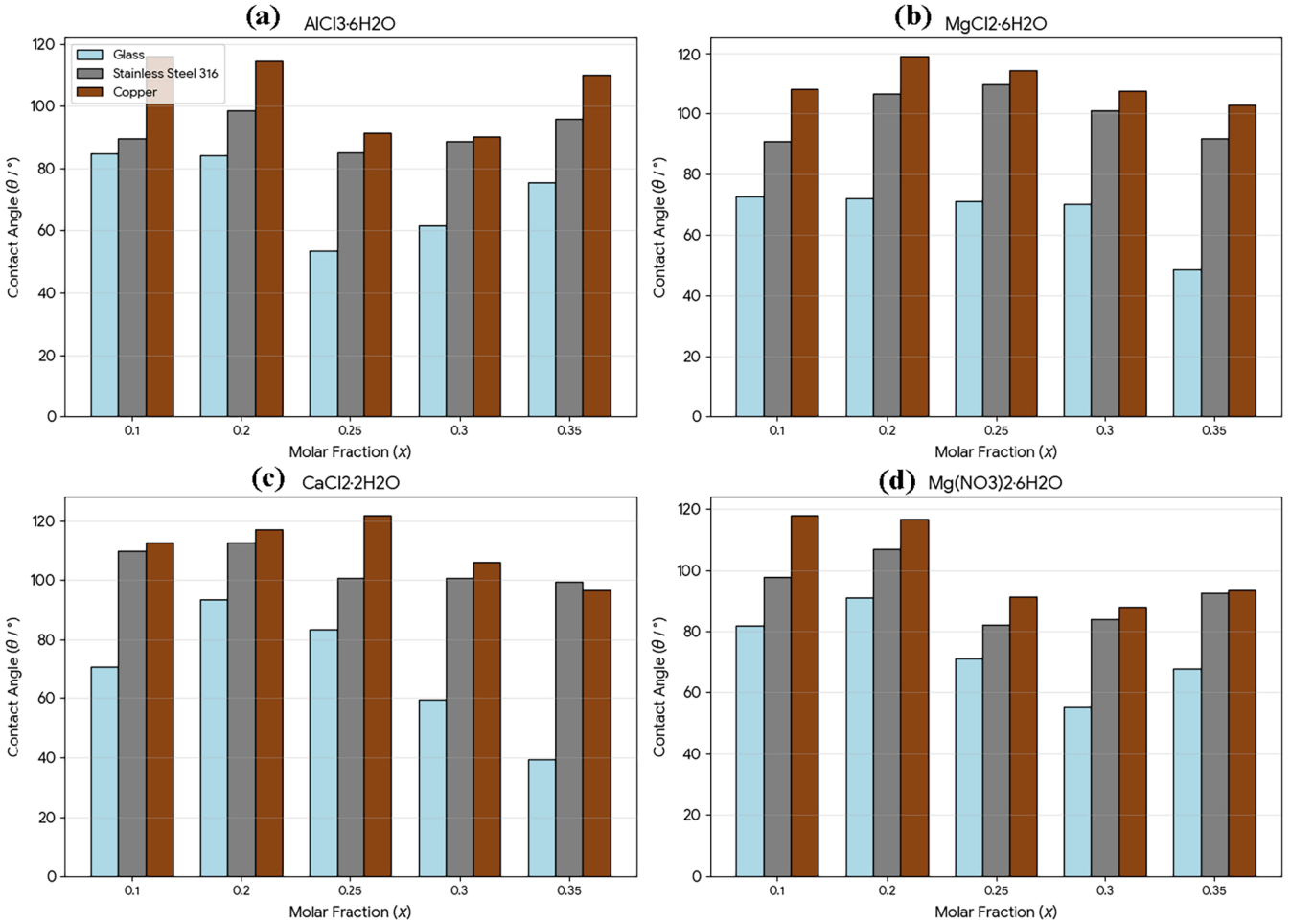

Figure 7. Experimental contact angle (θ) evolution for the studied DES families in this work as a function of the hydrated metal salt moles (n = 0.1 to 0.35). Each panel isolates a specific salt system (a) $AlCl_3.6H_2O$, (b) $MgCl_2.6H_2O$, (c) $CaCl_2.2H_2O$, and (d) $Mg(NO_3)_2.6H_2O$ to illustrate its composition-dependent wettability across three distinct solid substrates: glass, SS316, and copper at 298.15 K.

based DES such as ChCl:Gly:$AlCl_3$·$6H_2O$ (1:2:0.3, M6), with $\theta \approx 61°$ (Figure 6b).

In contrast, stainless steel 316 surfaces (Figure 6d,e) display consistently higher contact angles, indicating reduced wettability relative to glass. DESs containing magnesium nitrate hexahydrate, such as ChCl:Gly: Mg $(NO_3)_2$·$6H_2O$ (1:2:0.25, M24), exhibit θ values around 82° (Figure 6d), while calcium chloride-based DESs (M17) show significantly higher contact angles exceeding 110° (Figure 6e). Copper surfaces exhibit the poorest wetting behavior among the studied substrates (Figure 6f). For example, ChCl:Gly:$CaCl_2$·$2H_2O$ (1:2:0.25, M18)

Downloaded from pubs.acs.org/jceaax/article-pdf/71/7/2914/6510546/acs.jced.6c00151.pdf by UNIV DE BURGOS user on 07 September 2026

https://doi.org/10.1021/acs.jced.6c00151
J. Chem. Eng. Data 2026, 71, 2914–2931

displays a contact angle of approximately 122°, indicating limited spreading and weak liquid−solid interactions.

As illustrated in Figure 7, a consistent hierarchy of wettability is observed across all four DES systems on the basis of the nature of the solid substrate. Glass shows the lowest contact angles (most favorable wetting), followed by stainless steel 316, and finally copper (least favorable wetting). This sequence is a direct consequence of the substrate's surface free energy. The borosilicate glass surface is densely populated with highly polar silanol (−OH) groups that readily participate in the extended hydrogen-bonding network of the DES, promoting a high specific work of adhesion. Conversely, metallic substrates rely on their native passivation layers. These oxides are significantly less polar, relying primarily on weaker dispersive forces and limited ion−dipole interactions, which resist the spreading of the highly cohesive DES droplet.

Examining the specific salt systems in Figure 7, the aluminum and magnesium chloride DESs demonstrate remarkably stable, composition-dependent wetting behavior. Because the Al^{3+} and Mg^{2+} cations induce strong electrostriction and high bulk cohesive energy, their contact angles are generally moderate to high. However, a distinct trend emerges on the nonpolar metallic substrates: as the molar fraction of the salt increases toward n = 0.35, the contact angle incrementally decreases. This suggests that achieving a higher local charge density at the solid−liquid interface helps to overcome the weak dispersive interactions of the native metal oxides, marginally improving adhesion. Diverging from this behavior, the $CaCl_2$ system exhibits the most dramatic and anomalous wetting response in the data set. On the highly polar glass substrate, increasing the calcium concentration triggers a precipitous drop in the contact angle, reaching an exceptional spreading regime (θ∼39° at n = 0.35). Yet, on the less polar steel and copper surfaces, the exact same DES compositions become highly nonwetting, frequently exceeding. This severe divergence confirms that the complex, which exhibits the lowest bulk surface tension, possesses a high degree of conformational flexibility. It acts almost as an interfacial modifier, partitioning highly favorably at strongly polar boundaries like glass while being severely repelled by nonpolar metallic oxides. Finally, the substitution of the chloride anion for the nitrate anion introduces a notable shift in interfacial affinity. While it maintains the general substrate hierarchy, its contact angles on stainless steel 316 are distinctly suppressed and more stable across all concentrations compared to its chloride counterpart ($MgCl_2$). This indicates that the planar, delocalized geometry of the anion possesses a superior specific affinity for the chromium oxide passivation layer, demonstrating that wettability in ternary DES can be rationally tuned not only through cation valency but also via anion selection.

A qualitative correlation between surface tension and wettability is observed, as DESs with lower surface tension (γ) tend to exhibit smaller contact angles across all substrates. However, the relationship is not strictly linear, as reflected by the variability in θ values across DES families and substrates shown in Figures 6 and 7. These results highlight the important role of solid−liquid interfacial interactions, salt identity, and DES composition in governing wetting behavior beyond γ alone. Consequently, both γ and θ must be considered when evaluating DES performance in solid−liquid interfacial applications. From a practical perspective, surface tension and contact angle provide quantitative insight into wettability and liquid−solid interactions. Lower contact angle values indicate improved spreading over solid surfaces, while surface tension reflects the cohesive forces within the liquid. These properties are directly relevant to processes such as extraction, coating, and impregnation, where efficient contact between the solvent and solid substrate is required.

4. CONCLUSIONS

In this work, a systematic experimental characterization of the thermophysical and interfacial properties of choline chloride/glycerol (1:2) incorporating hydrated metal salts was carried out. Density, viscosity, speed of sound, surface tension, and contact angle were measured over a temperature range of 293.15 to 343.15 K, with varying metal salt concentrations. The results show that the incorporation of hydrated metal salts significantly modifies the physical behavior of glyceline, reflecting enhanced intermolecular interactions and increased structural organization within the liquid phase. Density and viscosity increase with metal salt content and decrease with temperature, while speed-of-sound measurements reveal systematic changes in compressibility and cohesive energy density, highlighting the nonideal nature of these mixtures. Empirical correlations were successfully applied to density, viscosity, and speed-of-sound data, accurately reproducing their temperature dependence and providing reliable mathematical descriptions suitable for modeling and process calculations. The proposed correlations accurately reproduce the experimental data and offer practical predictive capabilities for process modeling and design. Surface tension and contact angle measurements further elucidate the interfacial behavior of these DESs. The observed surface tension values and wettability trends depend on both metal salt identity and concentration, indicating that ion−solvent and solvent-surface interactions play a key role in determining liquid−solid interfacial properties. Differences in the contact angle across glass, stainless steel, and copper surfaces demonstrate the tunability of wettability in these systems, which is relevant for applications involving coating, impregnation, and biomass processing.

Overall, this work provides a comprehensive and coherent thermophysical and interfacial property data set for choline chloride/glycerol/metal salt hydrated DES. In this context, the present work provides a consistent and comparative data set that enables direct evaluation of how hydrated metal salts modify both bulk and interfacial properties relative to well-established binary systems. The combined analysis of bulk and interfacial properties contributes to a deeper understanding of structure−property relationships in complex DES systems and supplies reliable reference data to support solvent design and the development of DES-based industrial processes.

AUTHOR INFORMATION

Corresponding Authors

Gustavo A. Iglesias-Silva − *Departamento de Ingeniería Química, Tecnológico Nacional de México-Instituto Tecnológico de Celaya, Celaya, Guanajuato, C.P. 38010, México;* orcid.org/0000-0001-7260-2308; Email: gais@iqcelaya.itc.mx

Mert Atilhan − *Department of Chemical and Paper Engineering, Western Michigan University, Kalamazoo, Michigan 49008, United States;* orcid.org/0000-0001-8270-7904; Email: mert.atilhan@wmich.edu

Downloaded from pubs.acs.org/jceaax/article-pdf/71/7/2914/6510546/acs.jced.6c00151.pdf by UNIV DE BURGOS user on 07 September 2026

https://doi.org/10.1021/acs.jced.6c00151
J. Chem. Eng. Data 2026, 71, 2914−2931

Authors

Guadalupe Pérez-Durán − *Department of Chemical and Paper Engineering, Western Michigan University, Kalamazoo, Michigan 49008, United States;* orcid.org/0009-0002-2123-7253

Hamza I. Hossain − *Department of Chemical and Paper Engineering, Western Michigan University, Kalamazoo, Michigan 49008, United States*

Enrique Muñoz-Quintana − *Departamento de Ingeniería Química, Tecnológico Nacional de México-Instituto Tecnológico de Celaya, Celaya, Guanajuato, C.P. 38010, México*

Luis Antonio Castillo-Felix − *Departamento de Ingeniería Química, Tecnológico Nacional de México-Instituto Tecnológico de Celaya, Celaya, Guanajuato, C.P. 38010, México*

Supti Paul − *Department of Chemical and Paper Engineering, Western Michigan University, Kalamazoo, Michigan 49008, United States*

Santiago Aparicio − *Department of Chemistry, University of Burgos, Burgos 09001, Spain;* orcid.org/0000-0001-9996-2426

Alberto Gutiérrez-Vega − *Department of Chemistry, University of Burgos, Burgos 09001, Spain;* orcid.org/0000-0003-2000-7413

Complete contact information is available at: https://pubs.acs.org/10.1021/acs.jced.6c00151

Author Contributions

G.P.-D.: Conceptualization, data curation, formal analysis, investigation, methodology, visualization, and writing original draft; H.I.H.: data curation and investigation; E.M.-Q.: data curation and investigation; L.A.C.-F.: data curation and investigation; S.P.: data curation and investigation; S.A.: conceptualization and methodology; A.G.-V.: conceptualization and methodology; G.A.I.-S.: conceptualization, data curation, formal analysis, investigation, methodology, project administration, writing—original draft, and writing−review and editing; M.A.: conceptualization, data curation, formal analysis, investigation, methodology, project administration, writing−original draft, and writing−review and editing.

Notes

The authors declare no competing financial interest.

REFERENCES

(1) Peyrovedin, H.; Haghbakhsh, R.; Duarte, A. R. C.; Raeissi, S. A Global Model for the Estimation of Speeds of Sound in Deep Eutectic Solvents. *Molecules* **2020**, *25* (7), No. 1626.

(2) Abbott, A. P.; Boothby, D.; Capper, G.; Davies, D. L.; Rasheed, R. K. Deep Eutectic Solvents Formed between Choline Chloride and Carboxylic Acids: Versatile Alternatives to Ionic Liquids. *J. Am. Chem. Soc.* **2004**, *126* (29), 9142−9147.

(3) Deep Eutectic Solvents Formed between Choline Chloride and Carboxylic Acids: Versatile Alternatives to Ionic Liquids | Journal of the American Chemical Society. https://pubs.acs.org/doi/10.1021/ja048266j. (accessed January 20, 2026).

(4) Brett, C. M. A. Deep Eutectic Solvents and Applications in Electrochemical Sensing. *Curr. Opin. Electrochem.* **2018**, *10*, 143−148.

(5) Sun, X.; Zhou, Z.; Tian, D.; Zhao, J.; Zhang, J.; Deng, P.; Zou, H.; Lu, C. Acidic Deep Eutectic Solvent Assisted Mechanochemical Delignification of Lignocellulosic Biomass at Room Temperature. *Int. J. Biol. Macromol.* **2023**, *234*, No. 123593.

(6) Fernandes, C.; Melro, E.; Magalhães, S.; Alves, L.; Craveiro, R.; Filipe, A.; Valente, A. J. M.; Martins, G.; Antunes, F. E.; Romano, A.; Medronho, B. New Deep Eutectic Solvent Assisted Extraction of Highly Pure Lignin from Maritime Pine Sawdust (*Pinus Pinaster* Ait.). *Int. J. Biol. Macromol.* **2021**, *177*, 294−305.

(7) Al-Bodour, A.; Alomari, N.; Liew, S. K.; Aparicio, S.; Springstead, J.; Atilhan, M. Experimental and Theoretical Insights into CO2 and N2 Capture Using Natural Hydrophobic Deep Eutectic Solvents at High Pressures. *ACS Omega* **2025**, *10* (23), 24675−24696.

(8) Moradi, F.; Bougie, F. A Review of the Application of Deep Eutectic Solvents for Metal Recovery from Diverse Secondary Sources. *J. Mol. Liq.* **2026**, *443*, No. 128903.

(9) Cai, T.; Qiu, H. Application of Deep Eutectic Solvents in Chromatography: A Review. *TrAC, Trends Anal. Chem.* **2019**, *120*, No. 115623.

(10) Troter, D. Z.; Todorović, Z. B.; Đokić-Stojanović, D. R.; Stamenković, O. S.; Veljković, V. B. Application of Ionic Liquids and Deep Eutectic Solvents in Biodiesel Production: A Review. *Renewable Sustainable Energy Rev.* **2016**, *61*, 473−500.

(11) Shah, P. A.; Chavda, V.; Hirpara, D.; Sharma, V. S.; Shrivastav, P. S.; Kumar, S. Exploring the Potential of Deep Eutectic Solvents in Pharmaceuticals: Challenges and Opportunities. *J. Mol. Liq.* **2023**, *390*, No. 123171.

(12) Marcus, Y. Unconventional Deep Eutectic Solvents: Aqueous Salt Hydrates. *ACS Sustainable Chem. Eng.* **2017**, *5* (12), 11780−11787.

(13) Negi, T.; Kumar, A.; Sharma, S. K.; Rawat, N.; Saini, D.; Sirohi, R.; Prakash, O.; Dubey, A.; Dutta, A.; Shahi, N. C. Deep Eutectic Solvents: Preparation, Properties, and Food Applications. *Heliyon* **2024**, *10* (7), No. e28784.

(14) Deep Eutectic Solvents (DESs) and Their Applications | Chemical Reviews. https://pubs.acs.org/doi/10.1021/cr300162p?utm. (accessed January 25, 2026).

(15) Halder, A. K.; Haghbakhsh, R.; Voroshylova, I. V.; Duarte, A. R. C.; Cordeiro, M. N. D. S. Density of Deep Eutectic Solvents: The Path Forward Cheminformatics-Driven Reliable Predictions for Mixtures. *Molecules* **2021**, *26* (19), No. 5779.

(16) Tariq, M.; Freire, M. G.; Saramago, B.; Coutinho, J. A. P.; Lopes, J. N. C.; Rebelo, L. P. N. Surface Tension of Ionic Liquids and Ionic Liquid Solutions. *Chem. Soc. Rev.* **2012**, *41* (2), 829−868.

(17) Chen, Y.; Chen, W.; Fu, L.; Yang, Y.; Wang, Y.; Hu, X.; Wang, F.; Mu, T. Surface Tension of 50 Deep Eutectic Solvents: Effect of Hydrogen-Bonding Donors, Hydrogen-Bonding Acceptors, Other Solvents, and Temperature. *Ind. Eng. Chem. Res.* **2019**, *58* (28), 12741−12750.

(18) Wu, K.-J.; Chen, Q.-L.; He, C.-H. Speed of Sound of Ionic Liquids: Database, Estimation, and Its Application for Thermal Conductivity Prediction. *AIChE J.* **2014**, *60* (3), 1120−1131.

(19) Haghbakhsh, R.; Keshtkari, S.; Raeissi, S. Simple Estimations of the Speed of Sound in Ionic Liquids, with and without Any Physical Property Data Available. *Fluid Phase Equilib.* **2020**, *503*, No. 112291.

(20) Yebra, F.; Zemánková, K.; Troncoso, J. Speed of Sound as a Function of Temperature and Pressure for Propane Derivatives. *J. Chem. Thermodyn.* **2017**, *109*, 117−123.

(21) Cavuoto, G.; Lago, S.; Albo, P. A. G.; Serazio, D. Speed of Sound Measurements in Liquid Methane at Cryogenic Temperatures between (130 and 162) K and at Pressures up to 10 MPa. *J. Chem. Thermodyn.* **2020**, *142*, No. 106007.

(22) Yadav, A.; Trivedi, S.; Rai, R.; Pandey, S. Densities and Dynamic Viscosities of (Choline Chloride + Glycerol) Deep Eutectic Solvent and Its Aqueous Mixtures in the Temperature Range (283.15−363.15) K. *Fluid Phase Equilib.* **2014**, *367*, 135−142.

(23) Sazali, A. L.; AlMasoud, N.; Amran, S. K.; Alomar, T. S.; Pa'ee, K. F.; El-Bahy, Z. M.; Yong, T.-L. K.; Dailin, D. J.; Chuah, L. F. Physicochemical and Thermal Characteristics of Choline Chloride-Based Deep Eutectic Solvents. *Chemosphere* **2023**, *338*, No. 139485.

Downloaded from pubs.acs.org/jceaax/article-pdf/71/7/2914/6510546/acs.jced.6c00151.pdf by UNIV DE BURGOS user on 07 September 2026

(24) Ibrahim, A.; Tshibangu, M. M.; Coquelet, C.; Espitalier, F. Ternary Choline Chloride-Based Deep Eutectic Solvents: A Review. *ChemEngineering* **2025**, *9* (4), No. 84.
(25) Hall, K. R.; Kirwan, D. J.; Updike, O. L. Reporting Precision of Experimental Data. *Educ. Chem. Eng.* **1975**, *9*, 24−30.
(26) Smith, E. L.; Abbott, A. P.; Ryder, K. S. Deep Eutectic Solvents (DESs) and Their Applications. *Chem. Rev.* **2014**, *114* (21), 11060−11082.
(27) Chirico, R. D.; Frenkel, M.; Magee, J. W.; Diky, V.; Muzny, C. D.; Kazakov, A. F.; Kroenlein, K.; Abdulagatov, I.; Hardin, G. R.; Acree, W. E.; Brenneke, J. F.; Brown, P. L.; Cummings, P. T.; de Loos, T. W.; Friend, D. G.; Goodwin, A. R. H.; Hansen, L. D.; Haynes, W. M.; Koga, N.; Mandelis, A.; Marsh, K. N.; Mathias, P. M.; McCabe, C.; O'Connell, J. P.; Pádua, A.; Rives, V.; Schick, C.; Trusler, J. P. M.; Vyazovkin, S.; Weir, R. D.; Wu, J. Improvement of Quality in Publication of Experimental Thermophysical Property Data: Challenges, Assessment Tools, Global Implementation, and Online Support. *J. Chem. Eng. Data* **2013**, *58* (10), 2699−2716.
(28) Pérez-Durán, G.; Iglesias-Silva, G. A.; Cano-Gómez, J. J.; Ramos-Estrada, M. Densities, Dynamic Viscosities, and Speed of Sound of Glyceline + 1-Alcohols (C2-C4) from 288.15 to 343.15 K at 0.1 MPa. *J. Chem. Thermodyn.* **2024**, *193*, No. 107264.
(29) Predicting the Surface Tension of Deep Eutectic Solvents: A Step Forward in the Use of Greener Solvents. https://www.mdpi.com/1420-3049/27/15/489. (accessed April 16, 2026).
(30) Zhang, Q.; Vigier, K. D. O.; Royer, S.; Jérôme, F. Deep Eutectic Solvents: Syntheses, Properties and Applications. *Chem. Soc. Rev.* **2012**, *41* (21), 7108−7146.
(31) Hammond, O. S.; Bowron, D. T.; Edler, K. J. The Effect of Water upon Deep Eutectic Solvent Nanostructure: An Unusual Transition from Ionic Mixture to Aqueous Solution. *Angew. Chem., Int. Ed.* **2017**, *56* (33), 9782−9785.
(32) Deep Eutectic Solvents (DESs) and Their Applications | Chemical Reviews. https://pubs.acs.org/doi/10.1021/cr300162p. (accessed April 16, 2026).
(33) Marcus, Y. Effect of Ions on the Structure of Water: Structure Making and Breaking. *Chem. Rev.* **2009**, *109* (3), 1346−1370.

Downloaded from pubs.acs.org/jceaax/article-pdf/71/7/2914/6510469/acs.jced.6c00151.pdf by UNIV DE BURGOS user on 07 September 2026

https://doi.org/10.1021/acs.jced.6c00151
J. Chem. Eng. Data 2026, 71, 2914−2931